Deliverable D3.5

Report on metal reuse as raw powder for Additive Manufacturing

Funded by the European Union

Views and opinions expressed are those of the author(s) only and do not necessarily reflect those of the European Union or CINEA. Neither the European Union nor the granting authority can be held responsible for them. This project has received funding from Horizon Europe research and innovation programme under Grant Agreement No.1069890

Feasible Recovery of critical raw materials through a new circular Ecosystem for a Li-Ion Battery cross-value chain in Europe

WP3 - Recycling & Materials Re-using Technologies for Li-Ion Batteries

D3.5 – Report on metal reuse as raw powder for Additive Manufacturing

Due date of deliverable
31/08/2024

Actual submission date:
30/08/2024

Organisation name responsible for this deliverable: CSIC

Dissemination Level

SEN	Sensitive	
PU	Public	X

Project Acronym
FREE4LIB

Project Start Date
01-09-2022

Duration
48 months

Grant Agreement No.
101069890

Project End Date
31-08-2026

Funded by the European Union

Views and opinions expressed are those of the author(s) only and do not necessarily reflect those of the European Union or CINEA. Neither the European Union nor the granting authority can be held responsible for them. This project has received funding from Horizon Europe research and innovation programme under Grant Agreement No.1069890

Disclaimer

Free4lib is an EU-funded project that has received funding from the European Union's Horizon Europe research and innovation programme under grant agreement no. 101069890. The sole responsibility for the content of this report lies with the authors. It does not necessarily reflect the opinion of the European Union. The European Commission is not responsible for any use that may be made of the information contained therein.

Versions

DATE	VERSION	AUTHOR	COMMENT
25/07/2024	1	CSIC	First draft of the document
30/07/2024	2	CSIC, EURECAT	Second draft of the document
01/08/2024	3	CSIC, EURECAT	Third draft of the document
13/08/2024	4	TORRECID, FRAUNHOFER, AVL	Revised document by internal reviewers
16/08/2024	5	CSIC, EURECAT	Final document

Contents

Funded by the European Union

Views and opinions expressed are those of the author(s) only and do not necessarily reflect those of the European Union or CINEA. Neither the European Union nor the granting authority can be held responsible for them. This project has received funding from Horizon Europe research and innovation programme under Grant Agreement No.1069890

Funded by the European Union

Views and opinions expressed are those of the author(s) only and do not necessarily reflect those of the European Union or CINEA. Neither the European Union nor the granting authority can be held responsible for them. This project has received funding from Horizon Europe research and innovation programme under Grant Agreement No.1069890

List of Abbreviations

ACRONYMS	DESCRIPTION
SLM	Selective Laser Melting
VIGA	Vacuum Inert Melting Gas Atomizer
AM	Additive Manufacturing

Funded by the European Union

Views and opinions expressed are those of the author(s) only and do not necessarily reflect those of the European Union or CINEA. Neither the European Union nor the granting authority can be held responsible for them. This project has received funding from Horizon Europe research and innovation programme under Grant Agreement No.1069890

1. Executive summary

This work is aligned in the consequence of the objectives of WP3: Screening technologies around LIBs recycling & remanufacturing and testing them at laboratory scale (TRL 3-4). This main objective includes the development of a robotic battery pack disassembly line - recovery of valuable materials (metal oxides, plastics and metals) from used LIBs by different recycling technologies. Re-use of materials: - Validate valorised materials for the Batt value chain. - Validate the use of recycled materials in alternative applications.

This report focuses on the recovery of valuable metals by recycling and reuse of aluminium and copper components from an electric vehicle battery housing for the production of powder suitable for Selective Laser Melting (SLM) Additive Manufacturing. The processes consisted of disassembling the battery to retain only the metal parts. These parts were characterised for chemical composition and then melted and atomised using a high-pressure gas atomiser and a centrifugal atomiser to produce spherical AlSi7, AlSi7Mg and Cu powder. The particle size distribution of the AlSi powders was measured and the fraction below 63 µm was used for SLM.

Different energy densities and scanning speeds were tested to minimise porosity in the 3D printed samples. Metallographic analysis using light microscopy and ImageJ software quantified porosity, while microhardness and tensile tests assessed mechanical properties. Despite the high iron (Fe) content in the recycled aluminium (0.3-0.85 wt%) from the battery pack housing, the optimised SLM parameters resulted in samples with a high density of 99.98%. The microstructure revealed a fine α-Al solid solution and a network Si phase, with mechanical properties comparable to commercial AlSi10Mg alloys.

This study demonstrates the feasibility of recycling aluminium and copper from electric vehicle battery cases for advanced manufacturing applications, specifically SLM, while achieving good results despite the high Fe content in the composition of the aluminium parts.

2. Scope

Within T3.6., Recycling of metals at laboratory scale, this report deals with the results obtained:

- Manual dismantling and characterisation of aluminium parts of battery cases.

Funded by the European Union

Views and opinions expressed are those of the author(s) only and do not necessarily reflect those of the European Union or CINEA. Neither the European Union nor the granting authority can be held responsible for them. This project has received funding from Horizon Europe research and innovation programme under Grant Agreement No.1069890

- Melting and atomisation using two technologies, vacuum inert gas melting atomisation and centrifugal atomisation, to produce raw powder for additive manufacturing.
- Powder characterisation and classification
- Investigation and optimisation of powder processability for Selective Laser Melting Additive Manufacturing
- Evaluation of the 3D printed samples, micro-structure and mechanical properties and analysis of the effect of impurities in the scrap.

3. Introduction

The development of lighter electric vehicles (EVs) has gradually emerged as an important research priority due to its impact on energy consumption and greenhouse gas emissions [1]. The battery pack system (BPS), which is typically located at the bottom of the EV, accounts for a significant portion of the weight of an EV and thus has a significant influence on range, safety, and other important characteristics [2]. Obviously, there are two possible routes to improve the range with the battery pack system of an EV: increasing the energy density of the battery cells or reducing the weight of the battery pack enclosure (BPE) [3]. Improving the energy density of the battery cells is very challenging today due to the high energy densities already achieved and safety issues. It is therefore necessary to reduce the weight of the BPE in order to significantly improve performance [2]. To reduce the total weight of structural components, aluminium alloys are an advantageous choice due to the combination of low density and high impact resistance [4]. Typically, an EV battery of around 50 kW of energy has a weight of 340 kg of which only 210 kg is the weight of the cells [7]. The remaining weight is a majority combination of aluminium, with copper and steel. In other words, each EV battery pack is an invaluable source of recyclable aluminium [7].

Aluminium is a material with two well-known facets in terms of sustainability. On the one hand, the use of aluminium alloys reduces energy consumption in products and processes, such as lightweight shipping, packaging and construction, due to its low mass density. On the other hand, aluminium is one of the largest producers of greenhouse gases (GHG) and an energy-intensive industrial metal when produced from ore [8]. Therefore, secondary production through recycling and more efficient production of aluminium will make a significant contribution to achieving GHG reduction targets. Aluminium from primary production generates about 12-16.5 tonnes of GHG per tonne of metal, while aluminium alloys made entirely from scrap can reduce energy consumption and GHG emissions by > 90% [9].

Funded by the European Union

Views and opinions expressed are those of the author(s) only and do not necessarily reflect those of the European Union or CINEA. Neither the European Union nor the granting authority can be held responsible for them. This project has received funding from Horizon Europe research and innovation programme under Grant Agreement No.1069890

However, the use of aluminium scrap presents significant challenges in terms of sorting and tolerance to impurities in the secondary aluminium recovered. An increase in the use of scrap can be a source of compositional drift in the alloy streams [11]. Impurity tolerance is critical in aluminium alloy design because of the low solubility of many elements (except Mg and Zn) in aluminium, meaning that intermetallic phases form more easily with tramp element contamination than in many transition metal alloys. Minor changes in the solid solution state are commonly associated with relatively minor changes in properties, but a change in the present precipitates can be more disruptive, causing brittleness, corrosion or hydrogen embrittlement. Al-Mg-Si is a simple alloy system used, for example, in the production of automotive sheet, but when produced from scrap it becomes a complex multi-material containing iron, manganese, chromium, titanium, zinc and copper, impurities that can lead to brittle phases [12].

A study of automotive aluminium recycling found that it was difficult to produce wrought alloys from scrap, but identified cast alloys, Al-Si and 6082 alloy as the best production options from typical automotive wrought and cast alloys: 1xxx, 3xxx, 5xxx, 6xxx, 2xxx/7xxx/6xxx with Cu >1%, 4xxx, cast alloys (AlSi, AlMg) with low alloy/impurity contents (<0.5% for each) and cast alloys with high silicon content and higher alloy/impurity contents. The reason for this is that the ductile variants based on the Al-Mg and Al-Mg-Si systems are very sensitive to impurities, whereas many Al-Si alloys used for cast products are particularly tolerant to high scrap contents [11].

Specifically, Al-Si alloys are currently the most widely used aluminium alloy in additive manufacturing [4]. The potential of Additive Manufacturing (AM) to facilitate the reduction of anthropogenic greenhouse gas (GHG) emissions from the manufacturing industry is remarkable [13]. Even though AM is not inherently circular or sustainable, it can be an enabler for the sustainable development of new manufacturing scenarios [13]. AM can significantly reduce the consumption of raw materials and energy during the manufacturing process, and its distributed manufacturing system closer to the consumer reduces the carbon footprint by transporting raw materials and finished products over shorter distances [14]. In primary production, the embodied energy of bulk AlSi10Mg is around 189 MJ/kg, meanwhile the energy required to produce it by recycling is 32.7 MJ/kg and, interestingly, atomization to produce AlSi10Mg powder suitable for AM adds only an additional 8 MJ/kg to the embodied energy of the material [15]. This means that the need to produce the specific raw material in the form of micrometric spherical powder for AM does not significantly increase the energy cost associated with the production of the material.

Furthermore, the existing literature appears to indicate that many of the commercial aluminium alloys currently used for AM exhibit high impurity

Funded by the European Union

Views and opinions expressed are those of the author(s) only and do not necessarily reflect those of the European Union or CINEA. Neither the European Union nor the granting authority can be held responsible for them. This project has received funding from Horizon Europe research and innovation programme under Grant Agreement No.1069890

tolerance to Fe and other elements. This highlights the potential of using secondary aluminium as a feedstock for the production of aluminium-based powders for AM. Laser Powder Bed Fusion L-PBF, or Selective Laser Melting SLM, provides cooling rates on the order of 10^4 - 10^6 K/s, and fast solidification is recognised to increase the solubility of alloying elements in aluminium and reduce the size of secondary phase particles [16]. As a result, some of the mechanisms by which impurities have a detrimental effect on the properties of aluminium alloys can be reduced or even eliminated [17].

Suchy et al. [18] compared the microstructure and mechanical properties of AlSi9Cu3, an alloy commonly used in die cast automotive engine blocks. The alloy was produced by L-PBF and casting. The microstructure of the cast alloy contained 0.65 wt% Fe and was dominated by coarse eutectic Si and intermetallic phases rich in Fe and Cu. In contrast, the L-PBF processed material with a higher Fe content of 1.01 wt% had a significantly finer intermetallic dispersion and improved mechanical properties. Similar improvement in mechanical properties has been reported for AlSi12CuNiMg at nominal Fe concentrations of 0.1, 3 and 5% by L-PBF and casting [19]. The specimens were annealed at 300 °C with and without prior heat treatment to the T6 condition. Of the 300 °C annealed specimens, those produced by L-PBF exhibited improved strength and elongation at fracture in high temperature tensile tests at all Fe concentrations. The elongation at fracture also increased in the T6-treated additively produced samples, suggesting that Fe addition can improve the strength-ductility relationship in L-PBF processed Al-Si based alloys [19]. Fe improves the mechanical properties of AM alloys not only in the Al-Si system. By adding between 0.5 and 1 wt% Fe to Mn-modified wrought alloys of some 5xxx, 6xxx and 7xxx series alloys, increased tensile strength and elongation at break were achieved while reducing porosity and hot cracking susceptibility [20]. In addition, alloy 8009 (Al-8.5Fe-1.3V-1.7Si) when produced by L-PBF reaches an ultimate tensile strength of 454 MPa and an elongation at fracture of 7.2%, even the high Fe content due to not coarse intermetallic phases are formed [21].

These examples show that secondary aluminium alloys from recycled battery packs, with their sorting and impurity problems, could be excellent sources of AM powder. That is to say, high strength alloys for AM can be made with high concentrations of otherwise detrimental alloying elements. The aim of this work is to assess the possibility of recycling the different aluminium alloys from the frame and case of EV battery packs for the manufacture of powder by atomisation and their printability and characteristics for use in SLM.

Funded by the European Union

Views and opinions expressed are those of the author(s) only and do not necessarily reflect those of the European Union or CINEA. Neither the European Union nor the granting authority can be held responsible for them. This project has received funding from Horizon Europe research and innovation programme under Grant Agreement No.1069890

4. Battery case disassembling and pre-melting of the aluminium alloys recovered

The material used to produce the powder was obtained from a Hyundai Kona 64 kWh battery that had been removed due to a malfunction, discharged and disassembled by Accurec (Krefeld, Germany). Structural frames, covers, cooling plates and metal separators were manually disassembled and sent to the laboratory. Only the metal parts of the battery casing were retained. Visually similar parts were grouped and weighted.

The battery case studied consists of approximately 29.3 kg of steel (including 1.5 kg of fixings) and 45.5 kg of aluminium. This battery model consists of a steel lid and a cooled aluminium base with the cell modules mounted on aluminium frames. Figure 1 shows the manual process of disassembling the battery pack to extract the cell modules that was realised at Accurec.

The aluminium components are shown in Figure 2 and their elemental composition, measured by optical spark emission, and weight are given in Table 1 and Table 2. These parts consist of the module covers, the internal module separators, the case protectors, the battery cooling floor and the module support frames.

Figure 1. Original battery and different steps of its dismantling at Accurec.

Funded by the European Union

Views and opinions expressed are those of the author(s) only and do not necessarily reflect those of the European Union or CINEA. Neither the European Union nor the granting authority can be held responsible for them. This project has received funding from Horizon Europe research and innovation programme under Grant Agreement No.1069890

Table 1. Part type, quantity and weight breakdown of the battery case.

Part type a/ figure 2	Number of pieces	Weight per piece (kg)	Total weight (kg)
1, module covers	28	0.248	6.944
2, cells separators	390	0.036	14.040
3, case	1	0.245	0.245
4, case	1	0.415	0.415
5, cooling floor	2	2.100	4.200
6, cooling floor	6	2.100	12.600
7ª, frames	8	0.386	3.092
7B, frames	4	0.226	0.904
8, frames	4	0.770	3.080
			45.520

Table 2. Elemental composition (wt%) of part type according table 1 and figure 2.

	1	2	3	4	5	6	7A	7B	8
Si	11.66±0.35	0.12±0.01	0.13	0.15	0.26±0.01	0.15±0.01	0.55±0.01	0.63±0.02	0.53±0.01
Fe	0.56±0.02	0.29±0.02	0.74±0.02	0.55±0.01	0.85±0.05	0.70±0.04	0.41±0.01	0.47±0.03	0.30±0.01
Cu	0.40±0.01	0.04	0.10	0.05	0.13	0.15	0.07	0.07	0.06
Mn	0.55±0.02	0.030±0.002	0.98±0.08	1.14±0.03	1.09±0.04	1.01±0.03	0.06	0.06	0.08
Mg	0.29±0.01	1.68±0.05	0.91±0.03	0.90±0.01	<0.05	<0.05	0.49±0.02	0.39±0.01	0.47±0.01
Cr	-	0.021±0.001	-	-	-	-	-	-	-
Ni	0.03	-	-	-	-	-	-	-	-
Zn	0.79±0.02	0.030±0.003	0.030±0.001	0.022±0.001	0.036±0.002	0.028±0.001	0.077±0.005	0.051±0.002	0.070±0.002
Ti	0.11	0.022±0.002	0.019±0.001	0.016±0.001	0.027±0.002	0.022±0.001	0.035±0.001	0.038±0.001	0.034
Pb	0.09	-	-	-	-	-	-	-	-
Sn	0.04	-	-	-	-	-	-	-	-
Al	Base	Base	Base	Base	Base	Base	Base	Base	Base

Funded by the European Union

Views and opinions expressed are those of the author(s) only and do not necessarily reflect those of the European Union or CINEA. Neither the European Union nor the granting authority can be held responsible for them. This project has received funding from Horizon Europe research and innovation programme under Grant Agreement No.1069890

In light of the compositional results presented in Table 2, it can be reasonably inferred that parts initially classified separately, such as parts 3 and 4, 5 and 6, and 7 and 8, are likely to be composed of the same alloy or a similar alloy family. The battery case is constructed from a combination of five distinct aluminium alloys. The extreme covers of the modules are made from an AlSi12 casting alloy, while the internal module separators are produced using a 5xxx alloy. Two different 3xxx alloys are used for the thin cases and the cooling circuit plate, and finally, a 6xxx alloy is employed for the modules holding frames. Figure 3 illustrates the weight breakdown in percentage of the battery case in these alloys.

Funded by the European Union

Views and opinions expressed are those of the author(s) only and do not necessarily reflect those of the European Union or CINEA. Neither the European Union nor the granting authority can be held responsible for them. This project has received funding from Horizon Europe research and innovation programme under Grant Agreement No.1069890

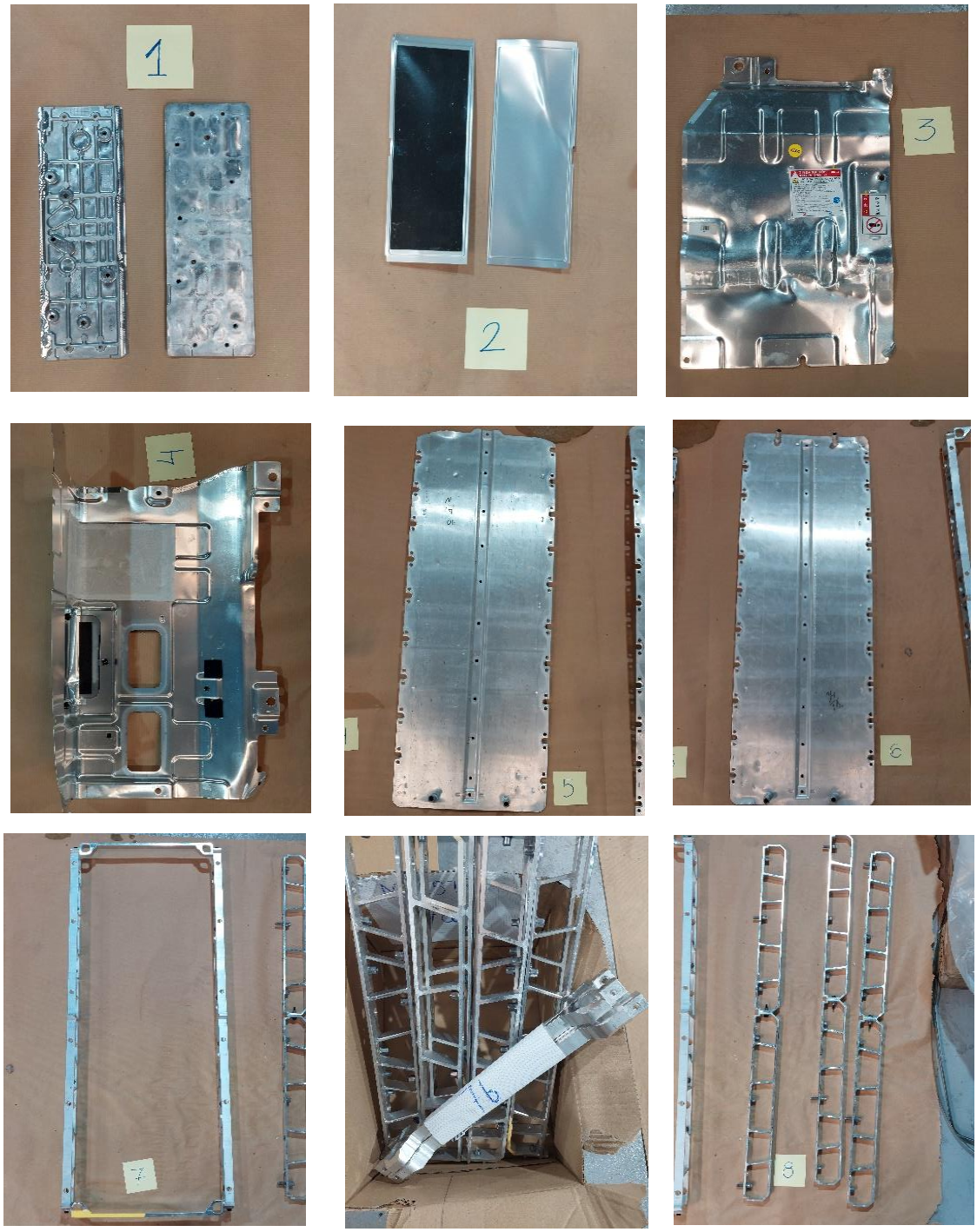

Figure 2. Classification of aluminium battery case parts a) module covers, b) separators, c) and d) case, e) and f) cooling floor, g), h) and i) frames.

Funded by the European Union

Views and opinions expressed are those of the author(s) only and do not necessarily reflect those of the European Union or CINEA. Neither the European Union nor the granting authority can be held responsible for them. This project has received funding from Horizon Europe research and innovation programme under Grant Agreement No.1069890

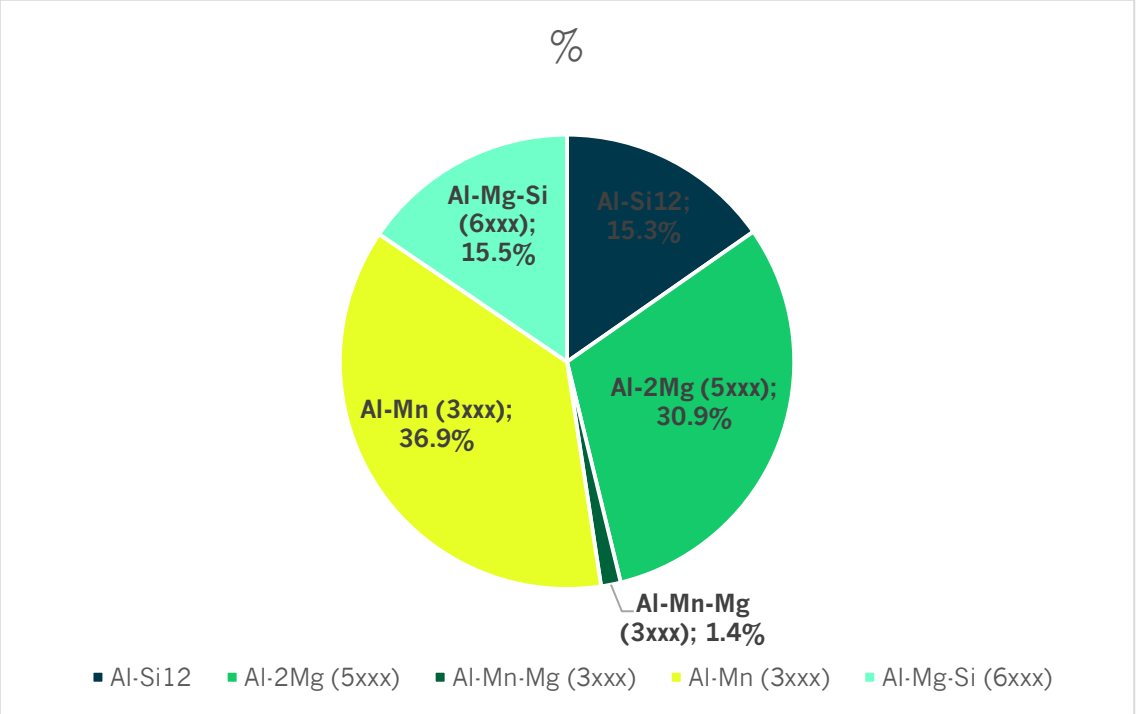

Figure 3. Battery case aluminium alloys weight breakdown

All the parts were cut with the appropriate tool, either shears or sheet metal shears, depending on the thickness of the metal sample. This was done until practical fragments were obtained, of a size that would subsequently allow the largest possible quantity of sample to be placed in a crucible for melting. In the case of the Type 2 parts, it was first necessary to remove the rubber covering one of their faces. This was achieved by immersing the metal sheets in acetone at room temperature until the adhesive was detached. For pieces 5 and 6, it was necessary to remove a film of polystyrene adhered to them and to clean the adhesive residue with acetone.

Components with comparable compositions were selected for casting in a single batch. The melting process was conducted in an electric furnace under aerobic conditions at a temperature of 750°C. During the melting process, smelting salts were added to the crucible to act as a flux and to protect the metal from oxidation. The smelting salts used in the recycling process are primarily sodium chloride (NaCl) and potassium chloride (KCl), with the addition of fluorides. The salt plays a vital role in the process, serving four primary functions. First, it breaks down the surface oxide layer, allowing for better metal adhesion. Second, it absorbs non-metallic impurities, preventing their adverse impact on the metal. Third, it protects the liquid metal from oxidation by forming a protective layer, and fourth, it enhances the precipitation of metal, improving its setting quality. The total weight of the ingots produced was 36.249 kg. The weight difference of -16.4% from the initial

Funded by the European Union

Views and opinions expressed are those of the author(s) only and do not necessarily reflect those of the European Union or CINEA. Neither the European Union nor the granting authority can be held responsible for them. This project has received funding from Horizon Europe research and innovation programme under Grant Agreement No.1069890

weight of all parts is due to the formation of slag and debris left in the crucible and moulds.

A total of 15 kg of the separately melted parts were sent to Eurecat, with the breakdown shown in Table 3, to produce powders by centrifugal atomisation, see point 7.

Table 3. Melted material supplied to Eurecat (Kg)

F-1	F-2	F-3+4	F-5+6	F-7	F-8
2.4	4.2	0.2	5.9	1.3	0.9

5. Selection of the target composition of powder

AlSi10Mg is the most commonly used aluminium alloy in AM. The literature review offers a comprehensive overview of the findings from various research papers on the different aspects of the Selective Laser Melting (SLM) AlSi10Mg aluminium alloy. The SLM process has attracted significant interest from researchers, with a focus on key printing parameters, optimisation methods, mechanical properties and microstructure of non-heat treated and heat treated AlSi10Mg alloy specimens. or a comprehensive and up-to-date review of this subject, refer to the work of R.E. Gite and C.D. Wakchaure [22].

In this project, we have selected a 7% wt Si aluminium alloy as the target for producing powder for SLM. AlSi7 is also a hypoeutectic alloy, with a silicon content of less than 11% by weight. It shares many characteristics with AlSi10Mg. Given that the alloy obtainable with the materials of this battery case has only 2% silicon, it was decided that an AlSi7 alloy would be the optimal solution, reducing the amount of additional silicon needed to add to the recovered aluminium from the battery pack parts. Magnesium, in conjunction with copper, plays a pivotal role in the hardening of cast aluminium alloys during heat treatment. The addition of magnesium increases the degree of precipitation hardening. However, it also promotes the formation of the π-AlFeMgSi phase ($Al_5Si_6Mg_5Fe_2$), an intermetallic rich in Fe, which can cause embrittlement of the AlSi alloys [23]. Furthermore, the formation of this phase reduces the amount of Si and Mg in solution, thereby reducing the age hardening capacity unless a homogenisation treatment at high temperature is performed [24]. Given the higher Fe content in the recycled alloys (0.3-0.85 wt%), which is above the typical amount in AlSi commercial powders for SLM (< 0.25 wt%), a low Mg AlSi7 alloy was selected as the target. With a lower Mg amount, the alloy is expected to exhibit a lower yield strength and strain hardening, but a higher elongation and ductility [25].

Funded by the European Union

Views and opinions expressed are those of the author(s) only and do not necessarily reflect those of the European Union or CINEA. Neither the European Union nor the granting authority can be held responsible for them. This project has received funding from Horizon Europe research and innovation programme under Grant Agreement No.1069890

6. Metal powder production using Vacuum Induction Melting Inert Gas Atomization

6.1 Introduction

Vacuum Induction Melting Inert Gas Atomisation or VIGA is one of the leading powder manufacturing processes for the production of large quantities of spherical, high quality metal powders. VIGA is characterised by process reliability, good productivity and low operating costs and is a flexible, state-of-the-art production method. The VIGA system allows to consistently produce high quality spherical particles with low oxygen concentration. In addition, produced powders have high purity, good flowability and the possibility to define the particle size distributions (PSDs).

Vacuum Induction Melting atomization process is easily scalable from lab scale (< 5 kg) to medium or industrial production (> 2000 kg). The main applications for additive manufacturing powders produced using VIGA technology are in the aerospace, medical and industrial gas turbine (IGT) industries. VIGA is suitable for the production from nickel superalloys, cobalt chrome powders, tool steels, or stainless steels to aluminium alloys.

6.2 Vacuum Induction Melting Inert Gas Atomizer description

The VIGA system integrates a vacuum induction melting unit with an inert gas atomisation unit. The starting materials are melted by means of electromagnetic induction, where electrical energy is coupled into the crucible/material under vacuum or inert gas atmosphere. Once the desired melt homogeneity and chemical composition is achieved, the crucible is tilted into a gravity feeder. The fine metal stream flowing from the orifice of the melting funnel into the atomising nozzle system is subjected to a high-pressure jet of inert gas and then atomised. The combination of molten metal and gas jet creates a spray of micro-droplets which solidify in the atomisation tower to form a fine, spherical powder. Figure 4 shows a scheme and Figure 5 shows the VIGA equipment available at CSIC and used for the powder production.

Funded by the European Union

Views and opinions expressed are those of the author(s) only and do not necessarily reflect those of the European Union or CINEA. Neither the European Union nor the granting authority can be held responsible for them. This project has received funding from Horizon Europe research and innovation programme under Grant Agreement No.1069890

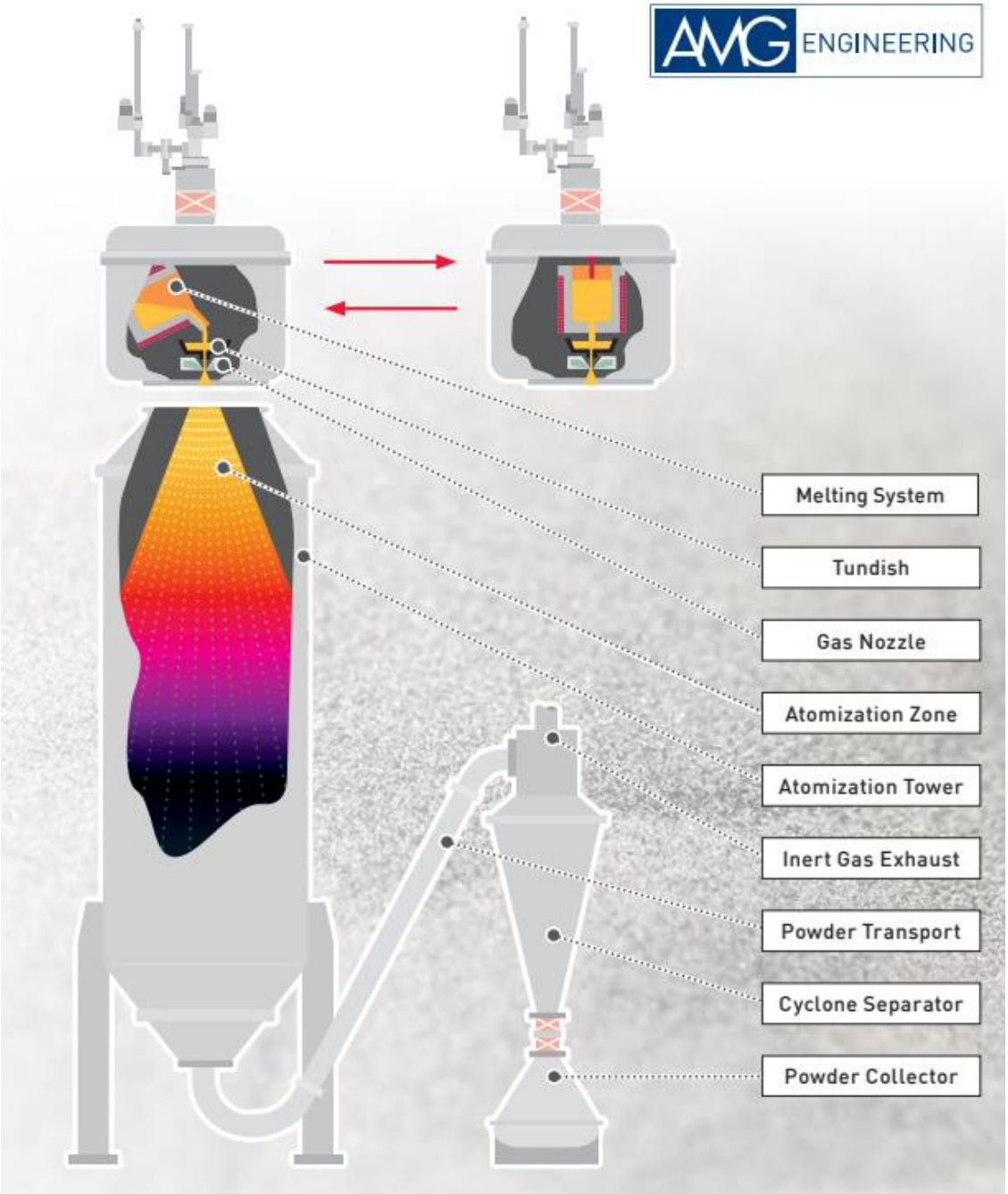

Figure 4. VIGA scheme from ALD Vacuum Technologies (https://www.ald-vt.com/)

Funded by the European Union

Views and opinions expressed are those of the author(s) only and do not necessarily reflect those of the European Union or CINEA. Neither the European Union nor the granting authority can be held responsible for them. This project has received funding from Horizon Europe research and innovation programme under Grant Agreement No.1069890

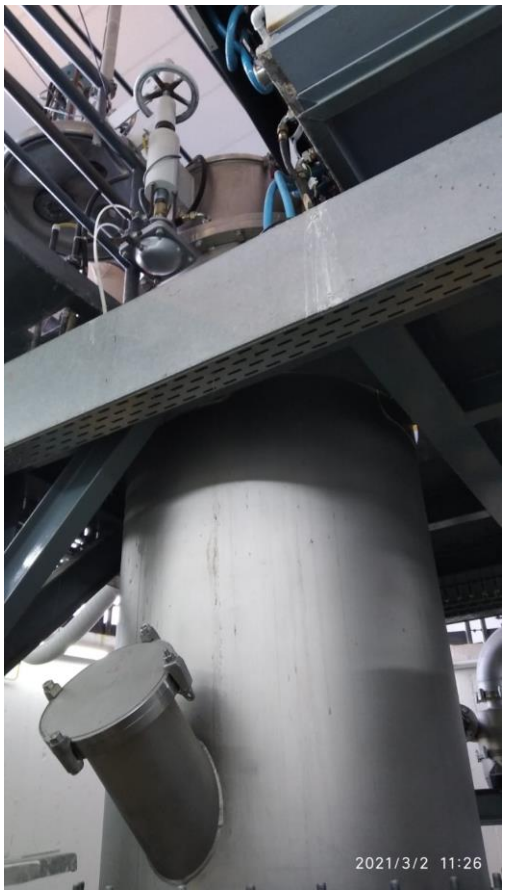

Figure 5. VIGA equipment used at the CSIC for the production of powder

6.3 Set-up of atomizer

An appropriate proportion of the different pre-melted ingots were then mixed and atomised in a high-pressure gas atomiser with confined nozzle (Leybold VIGA 2S) at CSIC. Argon was used as the inert gas at a pressure of 22-25 bar. Accordingly, the atomiser crucible was loaded with 5 kg of aluminium, derived from the addition of 1.100 kg of AlSi20 mother alloy to 3.900 kg of ingots produced through the pre-melting of battery case components. The total weight of the argon atomised powder collected was 4.470 kg.

6.4 Characterization of the produced powders

The particle size distribution (PSD) of the resulting powder was measured using the laser diffraction method with the powder dispersed in isopropyl alcohol. The resulting powder has a volume distribution centred on a diameter of approximately 50 µm, as illustrated in Figure 6. To eliminate the excessively large powder and conduct a detailed analysis of the size distribution, the powder was sieved into the fractions outlined in Table 4. The optimal fraction

Funded by the European Union

Views and opinions expressed are those of the author(s) only and do not necessarily reflect those of the European Union or CINEA. Neither the European Union nor the granting authority can be held responsible for them. This project has received funding from Horizon Europe research and innovation programme under Grant Agreement No.1069890

for SLM, with a diameter of less than 63 µm, corresponds to 1.125 kg, which is 25.2% of the total powder obtained. The fraction between 63 and 150 µm, representing 1,829 kg, could be used directly for other AM technologies such as Direct Energy Deposition (DED) [26]. An alternative option would be to re-atomise the powder along with the remaining ingots. It should be noted that the objective of this study is not to optimise the atomisation parameters, such as melt overtemperature or argon pressure. Therefore, standard parameters for aluminium alloys have been used. Further optimisation of the atomisation process could result in a higher yield of powder sizes below 63 µm [27].

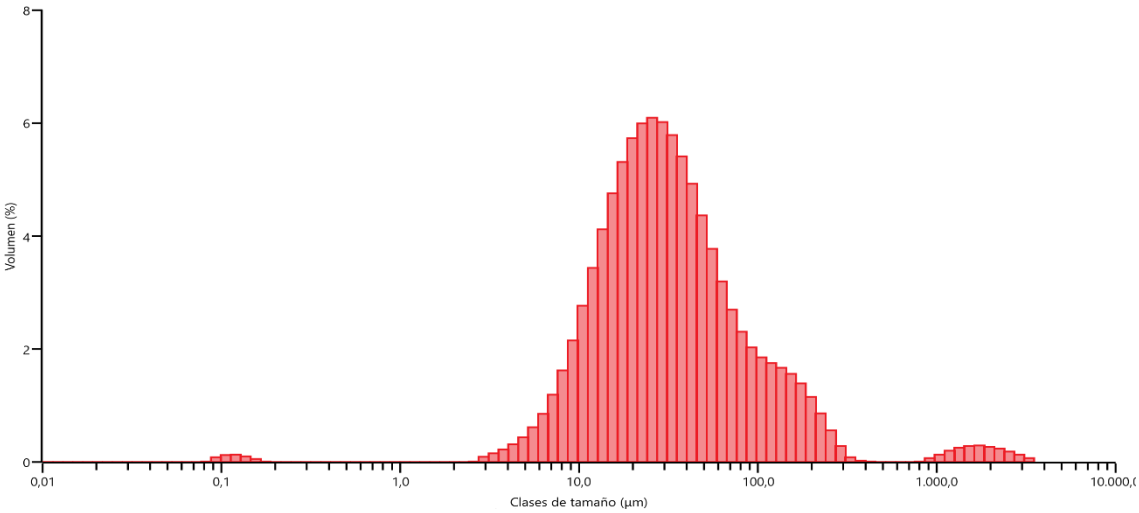

Figure 6. Particle Size Distribution of the obtained AlSi7 powder.

Table 4. Weight obtained from each fraction of sieved powder.

Size diameter fraction (µm)	Weight (g)
>250	364.36
150-250	1009.96
100-150	1363.50
63-100	466.54
<63	1125.37

The powder fraction smaller than 63 µm was subjected to further analysis following sieving, resulting in the distribution illustrated in Figure 7. It is noted

Funded by the European Union

Views and opinions expressed are those of the author(s) only and do not necessarily reflect those of the European Union or CINEA. Neither the European Union nor the granting authority can be held responsible for them. This project has received funding from Horizon Europe research and innovation programme under Grant Agreement No.1069890

that a notable proportion of the powder exhibits dimensions below 20 µm, which is not typically found in commercial SLM powder. However, we retained these particles as a wider particle size distribution provides a higher powder bed density and generates higher density parts for a given energy input [28]. Furthermore, a bimodal powder distribution enables enhanced interaction with the laser beam and increased absorption by the bed, which is particularly advantageous for reflective powders such as aluminium [29]. Despite the powder being handled correctly and the appearance of the wiper spread layers being homogeneous, the powder fluidity was below the threshold for measurement by a Hall flowmeter funnel.

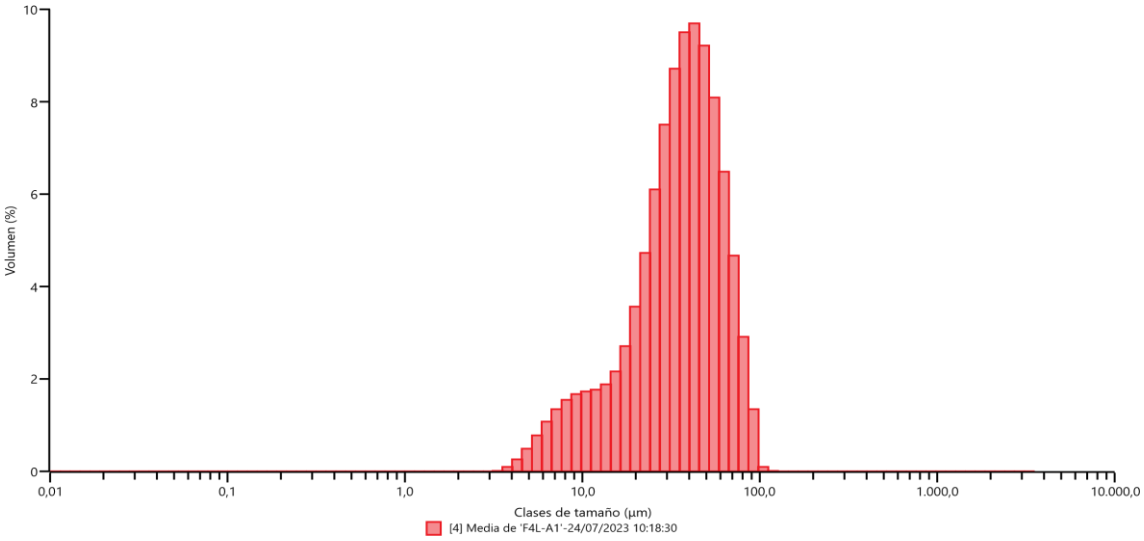

Figure 7. Particle Size Distribution of the sieved (<63 µm) AlSi7 powder.

Figure 8 depicts the powder's morphology, which is predominantly spherical with a certain proportion of non-spherical forms and satellites. The figure also displays a very wide size distribution. Figure 9 shows the image of the powder embedded in Bakelite, polished to reveal its internal structure. It also demonstrates that the presence of potential pores formed during solidification during atomisation is absent.

Funded by the European Union

Views and opinions expressed are those of the author(s) only and do not necessarily reflect those of the European Union or CINEA. Neither the European Union nor the granting authority can be held responsible for them. This project has received funding from Horizon Europe research and innovation programme under Grant Agreement No.1069890

Figure 8. Scanning electron microscope image of the powder fraction < 63 µm.

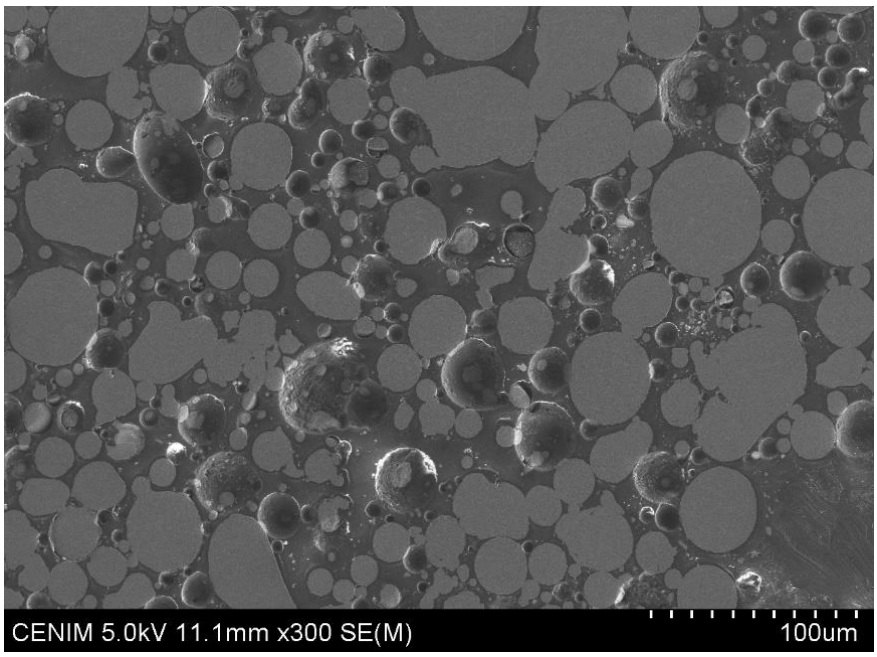

Figure 9. Scanning electron microscope image of the powder fraction < 63, mounted and polished to reveal the interior.

Funded by the European Union

Views and opinions expressed are those of the author(s) only and do not necessarily reflect those of the European Union or CINEA. Neither the European Union nor the granting authority can be held responsible for them. This project has received funding from Horizon Europe research and innovation programme under Grant Agreement No.1069890

6.5 Conclusions in powder production using VIGA atomization

A powder with a particle size distribution suitable for SLM, particularly in the < 63 µm range, was produced by inert gas atomisation of the recycled aluminium.

The morphology was predominantly spherical and the internal structure was free from any significant pores, indicating that the material is of a quality that is suitable for the purposes of AM.

The composition of the obtained parts reveals a higher proportion of Fe than that observed in SLM parts made from commercial powder. However, the as-built microstructure of the printed AlSi7 alloy demonstrated typical fine microstructures with distinct melt pool boundaries and the absence of detrimental AlSiFe precipitates. The mechanical testing demonstrated that the hardness values (105±5 HV) were slightly lower than those of AlSi10Mg due to the absence of magnesium. However, they were comparable to those of high-pressure die cast AlSi10Mg, and the ultimate tensile strength and % elongation values were within the range of those typically observed in SLM-produced AlSi alloys.

7. Metal powder production using centrifugal atomization

7.1 Introduction

This section details all the tasks related to testing centrifugal atomization for its use in recycling metals at a lab scale. It describes the setup for producing AlSi7Mg powders using recovered metal and the setup for producing Cu powders. Additionally, it outlines the characterization of the obtained powder. Several test runs were performed to produce AlSi7Mg under different conditions to optimize the process and to produce enough metal powder to be used in additive manufacturing in subsequent project tasks.

Funded by the European Union

Views and opinions expressed are those of the author(s) only and do not necessarily reflect those of the European Union or CINEA. Neither the European Union nor the granting authority can be held responsible for them. This project has received funding from Horizon Europe research and innovation programme under Grant Agreement No.1069890

7.2 Metal powder process set-up

7.2.1 Description of raw material

Raw materials from CSIC, Figure 10. Aluminum recovered by CSIC, were received and classified based on the original parts. Most of this material was collected and mixed in the quantities shown in Table 5.

Figure 10. Aluminum recovered by CSIC

Table 5. Raw aluminum used for manufacturing AlSi7Mg alloy.

Alloy	Material (kg)
F-1	1.92
F-2	3.37
F-3+4	0.14
F-5+6	4.73
F-7	1.05
F-8	0.722
Total	11.94

Based on the specific Si content and the quantity of each alloy, the resulting alloy weighed 11,94 kg and contained an average of 2,46% Si. To achieve the desired composition of the AlSi7Mg alloy with up to 7% Si, 1,26 kg of a 50%Al-50%Si master alloy was used to form the final AlSi7Mg alloy. Figure 11 shows the manufactured billets of AlSi7Mg alloy. Their dimensions fit the crucible dimensions, facilitating further processing.

Figure 11. Billets of AlSi7Mg produced at EUT facilities.

Funded by the European Union

Views and opinions expressed are those of the author(s) only and do not necessarily reflect those of the European Union or CINEA. Neither the European Union nor the granting authority can be held responsible for them. This project has received funding from Horizon Europe research and innovation programme under Grant Agreement No.1069890

For the Cu alloy, no metal stream was received due to the difficulty other partners faced in obtaining enough of the material. For this laboratory-scale test, scrap Cu metal from electrical wires was used.

7.2.2 Atomizer description

The production of powder by centrifugal atomization is achieved by melting material in a crucible and releasing it once it reaches its liquid state onto a metallic disc that rotates at high speeds. When the molten metal hits the spinning disc, it is atomized. Small particles are sprayed and projected from the disc into the surroundings where they are quickly cooled by contact with the inert gas inside the chamber.

Figure 12. Atomizer pilot plant.

The process takes place in the atomizer, a sealed cone-shaped metal chamber housing an electric motor in the centre, as shown in Figure 12. This motor is responsible for rotating the disc attached to its shaft. The atomizer has two openings, one at the top and one at the bottom. In the upper part, there is a lid to which a cooled platform is attached, accommodating the induction coil surrounding the crucible. The lower lid houses the deposit that collects the atomized powder.

7.2.3 Set-up of atomizer and runs

7.2.3.1 Atomization set-up for AlSi7Mg alloy

AlSi7 aluminium billets are deposited inside the alumina crucible as shown in Figure 13. It also contains the stopper covering the melt outlet hole located in

Funded by the European Union

Views and opinions expressed are those of the author(s) only and do not necessarily reflect those of the European Union or CINEA. Neither the European Union nor the granting authority can be held responsible for them. This project has received funding from Horizon Europe research and innovation programme under Grant Agreement No.1069890

the centre of the crucible and a thermocouple to control the temperature. The opening movement of the stopper is carried out by an electric actuator which raises the alumina stopper when atomization starts. The crucible assembly is located inside the induction coil which is connected to the inductor that supplies the electrical power. The disc used for these atomizations had a concave insert with a Zr_2O coating.

Figure 13. Alumina crucible filled with AlSi7 billets.

7.2.3.2 Atomization runs for AlSi7Mg alloy

Several atomizations of AlSi7Mg were carried out and their specifications are listed in Table 6. Similar amounts of material were atomized while keeping the same process parameters. The only variant introduced was the type of inert gas used for filling the chamber, to check the influence of this gas on the final atomized powder.

Table 6. Atomization runs for AlSi7Mg alloy.

At. Num.	Quantity (gr)	Temperature (C°)	Speed (rpm)	Gas
1	951.2	950	40000	Nitrogen
2	924.4	950	40000	Argon
3	928.9	950	40000	Nitrogen
4	955.8	950	40000	Argon
5	989.1	950	40000	Argon
6	953.7	950	40000	Nitrogen

Funded by the European Union

Views and opinions expressed are those of the author(s) only and do not necessarily reflect those of the European Union or CINEA. Neither the European Union nor the granting authority can be held responsible for them. This project has received funding from Horizon Europe research and innovation programme under Grant Agreement No.1069890

7.2.3.3 Atomization set-up for Cu alloy

For the atomization of the copper powder, cut copper wire has been used as raw material. A total of 1.750 g of copper filaments were placed in a crucible made of graphite where they were melted by means of induction currents. The stopper which closes the outlet hole of the molten metal in the crucible is also made of graphite. The disc used was a flat disc with an alumina ceramic coating. Atomization was carried out at a speed of 35.000 rpm in an inert nitrogen environment. The disc during the atomization process was water-cooled to resist the molten copper which was heated up to 1.300°C.

7.2.3.4 Atomization runs for Cu alloy

To produce the Cu powder, 3 different atomizations were carried out. The specifications for each of them are listed in Table 7. In all of them the melting temperature, disc velocity and inert gas were kept fixed.

It is important to notice that the performance of this atomization was far from being a stable atomization and an in-depth review of process parameters is required. Further development for this material will be performed during task T4.6.

Table 7. Atomization runs for Cu alloy.

At. Num.	Quantity (gr)	Temperature (C°)	Speed (rpm)	Gas
1	1750	1300	35000	Nitrogen

7.2.4 Summary of produced powders

The following Table 8 shows the summary of the powder granulometry obtained from the AlSi7Mg atomizations. The table lists the atomizations in chronological order and the quantities obtained as a function of particle size. The efficiency of particles fractions < 63 µm is also shown.

Table 8. Summary of produced AlSi7Mg powder

At. Num.	Quantity obtained by granulometry (g)				Total mass (g)	Efficiency (%)
	600-150 µm	150-106 µm	106-63 µm	<63 µm		<63 µm
1	32.73	15.30	38.60	18.86	105.50	17.88
2	107.09	128.85	174.40	53.07	463.43	11.45
3	74.88	100.07	126.71	31.36	333.02	9.42
4	78.98	84.54	110.88	30.18	304.59	9.91

Funded by the European Union

Views and opinions expressed are those of the author(s) only and do not necessarily reflect those of the European Union or CINEA. Neither the European Union nor the granting authority can be held responsible for them. This project has received funding from Horizon Europe research and innovation programme under Grant Agreement No.1069890

5	58.42	142.76	226.56	48.34	476.10	10.16
6	27.86	220.09	272.02	63.37	583.35	10.86

Similarly, Table 9, collects the atomized Cu powder quantities obtained by granulometry. Efficiency is also shown for less than 45 µm particle size.

Table 9. Summary of produced Cu powder

At. Num.	Quantity obtained by granulometry (g)				Total mass (g)	Efficiency (%)
	600-150 µm	150-75 µm	75-45 µm	<45 µm		<45 µm
1	48.77	821.8	541.9	239.75	165.,22	14.51

7.3 Characterization of produced powders

7.3.1 AlSi7Mg powder

Figure 14**¡Error! No se encuentra el origen de la referencia.** shows the SEM images of the AlSi7Mg powder. The atomized powder meets the requirements or qualities in morphology necessary for its use in additive manufacturing processes. It can be observed that the particles have a high degree of sphericity with almost no satellites, which will increase its flowability. In addition, in the image on the right (100x) it is noticeable the smooth surface they exhibit. All these factors make this powder suitable for printing.

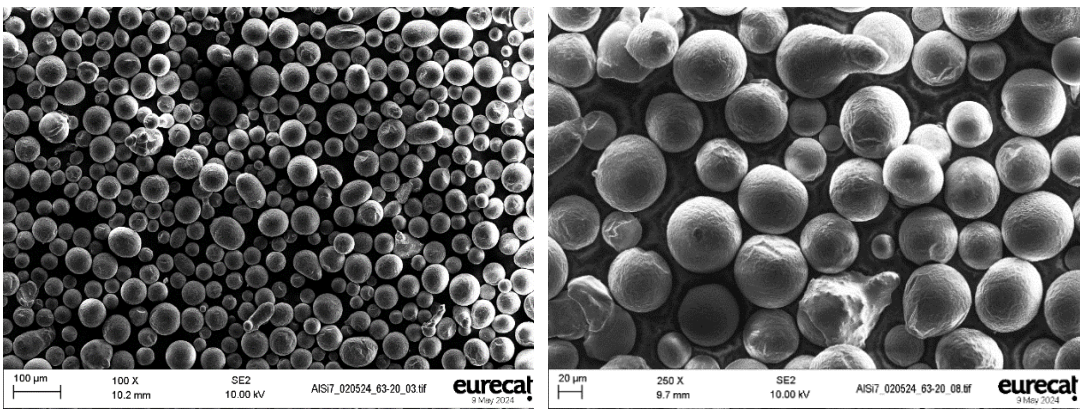

Figure 14. SEM images of AlSi7Mg powder (100x, 250x).

Figure 15 shows images taken of the AlSi7Mg powder with the optical microscope. After manual polishing the cross section reveals the characteristic dendritic microstructure of these particles. On the other hand, Figure 16 and Table 10 reveal the SEM-EDX for that powder specifying the amount in percentage of each one of the elements forming the particles.

Funded by the European Union

Views and opinions expressed are those of the author(s) only and do not necessarily reflect those of the European Union or CINEA. Neither the European Union nor the granting authority can be held responsible for them. This project has received funding from Horizon Europe research and innovation programme under Grant Agreement No.1069890

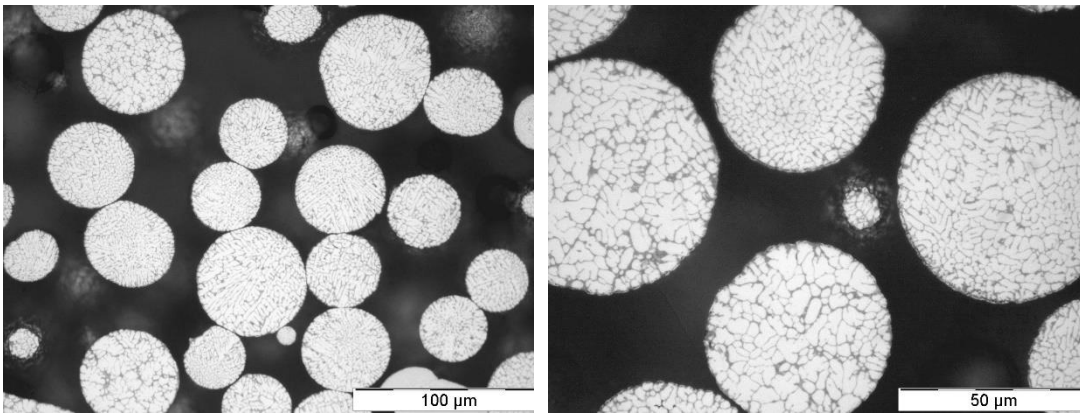

Figure 15. OM cross section images of AlSi7Mg (50x, 100x)

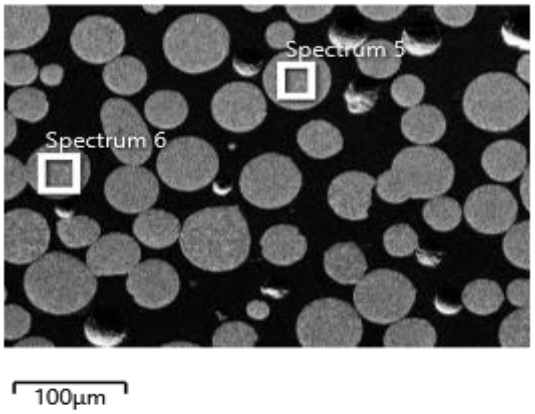

Figure 16. SEM-EDX 5results for AlSi7Mg.

Spectrum Label	Spectrum 6	Spectrum 5
Mg	-	0.59
Al	91.33	91.46
Si	8.67	795
Total	100	100

Table 10. SEM-EDX results for AlSi7Mg

Figure 17 illustrates the volume size distribution of powder particles as a function of their diameter for six different atomization and Figure 18 shows the cumulative distribution of particle diameters for the different atomizations. The x-axis shows particle diameters ranging from 1 µm to 1000 µm, on a logarithmic scale. The y-axis represents the volume size distribution as a percentage. Each curve has a peak indicating the most common particle size within each sample.

Funded by the European Union

Views and opinions expressed are those of the author(s) only and do not necessarily reflect those of the European Union or CINEA. Neither the European Union nor the granting authority can be held responsible for them. This project has received funding from Horizon Europe research and innovation programme under Grant Agreement No.1069890

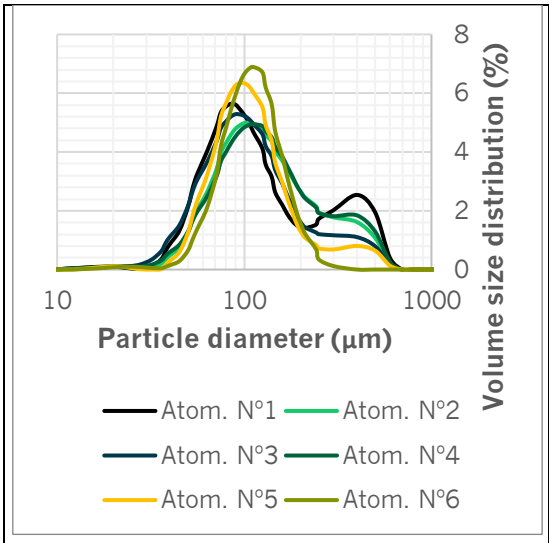

Figure 17. Volume size distribution plot.

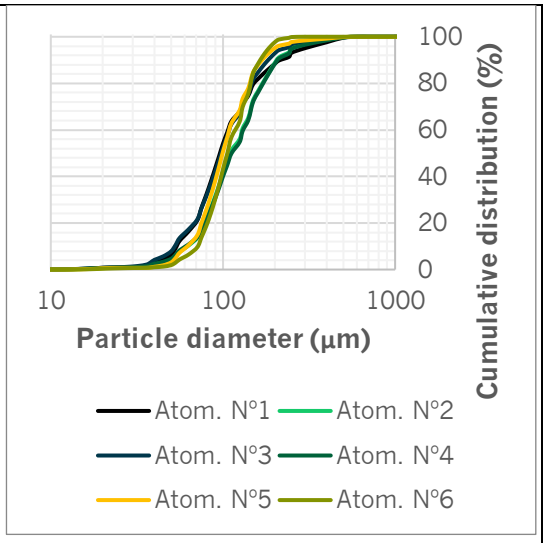

Figure 18. Cumulative distribution plot.

All samples show a primary peak around 100 µm range. Atom. N°1 and Atom. N°4 exhibit secondary peaks around the 400 µm. Atom. N°6 has a distinct peak, the highest among the samples, indicating a significant portion of particles around the primary peak size.

As a summary, Table 11 includes the cumulative distribution of the particles size calculated with the different reference points D10, D50 and D90, as well as the mean size for each atomization in microns.

Table 11. Cumulative distributions D10, D50, D90 and mean size [µm].

Atom. Num.	D10	D50	D90	Mean size
1	53.45	101.12	356.66	164.91
2	58.92	114.92	300.85	158.21
3	49.15	95.77	243.35	131.31
4	57.70	117.53	318.13	162.78
5	59.09	97.89	186.14	124.79
6	64.31	104.53	164.31	114.04

7.3.2 Cu powder

The following Figure 19 shows SEM images of the copper powder with particles ranging from 45 to 75 µm. These images reveal a high degree of sphericity of the particles, with a smooth surface and barely any satellites. On the other side, Figure 20 and Table 12 illustrate the composition of the powder from three different particles.

Funded by the European Union

Views and opinions expressed are those of the author(s) only and do not necessarily reflect those of the European Union or CINEA. Neither the European Union nor the granting authority can be held responsible for them. This project has received funding from Horizon Europe research and innovation programme under Grant Agreement No.1069890

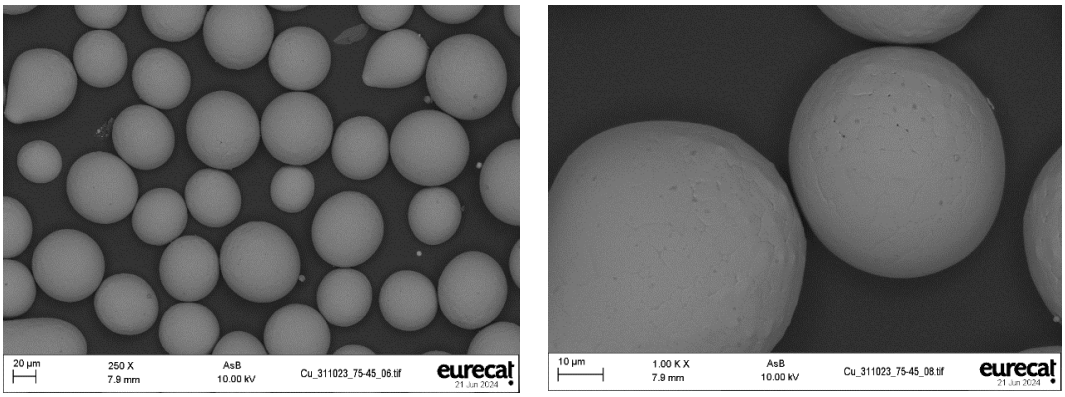

Figure 19. SEM results Cu powder.

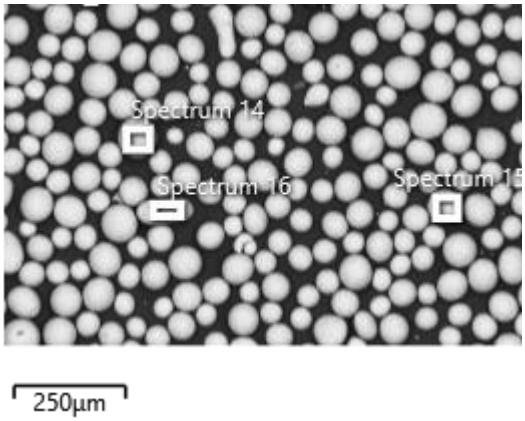

Figure 20. SEM-EDX results for Cu powder.

Spectrum Label	Spectrum 14	Spectrum 15	Spectrum 16
O	3.04	2.59	3.36
Cu	96.96	97.41	96.64
Total	100	100	100

Table 12. SEM-EDX results for Cu powder.

Cross section images of the Cu powder were also taken and are illustrated in Figure 21. From these OM images it is possible to observe the different grains present in those particles with their distinctive grain boundaries.

Figure 22 illustrates the volume size distribution and the cumulative distribution of Cu powder particles as a function of their diameter. In this graph it is clearly noticeable a primary peak around 90 µm range and no secondary peak.

Funded by the European Union

Views and opinions expressed are those of the author(s) only and do not necessarily reflect those of the European Union or CINEA. Neither the European Union nor the granting authority can be held responsible for them. This project has received funding from Horizon Europe research and innovation programme under Grant Agreement No.1069890

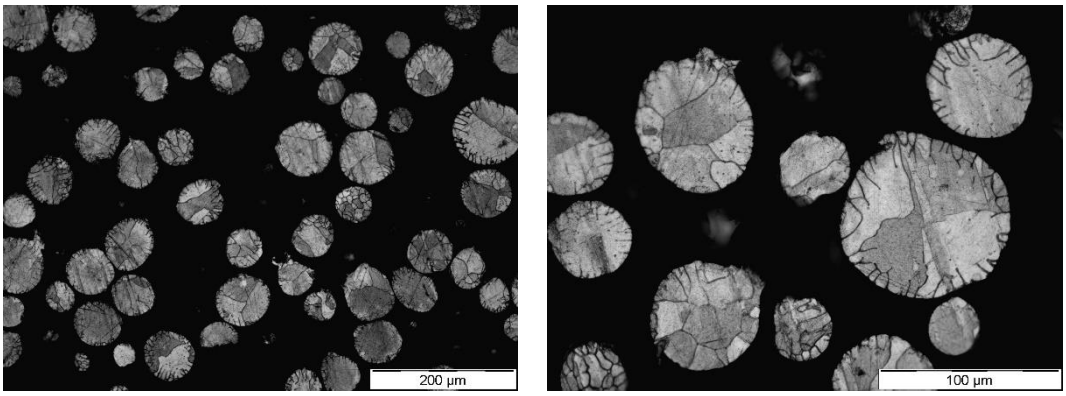

Figure 21. OM cross section images for Cu powder.

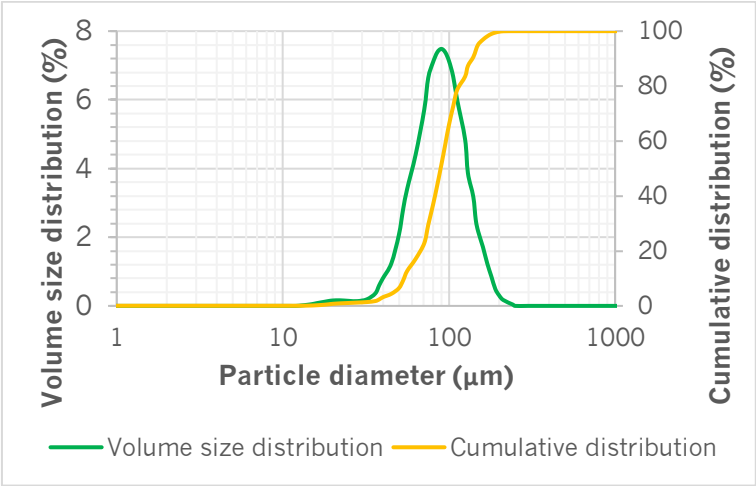

Figure 22. Volume and cumulative distributions for Cu powder.

7.4 Conclusions in powder production using centrifugal atomization

Regarding the AlSi7Mg powder, it was observed that the variation of the inert gas used to inert the atomizer chamber did not have a relevant impact on the powder produced. Since with both Ar and N_2 gases, similar yields were achieved in terms of powder obtained with a particle size of less than 63 µm. The quality obtained was practically the same since both cases showed spherical particles with a smooth outer surface and barely any satellites. Also, the atomization of AlSi7Mg powders is a stable process and results show that the technology for this alloy can be scalable.

However, for Cu alloys more trials are required to adjust de process to get a stable atomization. This development and more trial tests will continue in Task T4.6 to study the scalability for Cu alloys.

Funded by the European Union

Views and opinions expressed are those of the author(s) only and do not necessarily reflect those of the European Union or CINEA. Neither the European Union nor the granting authority can be held responsible for them. This project has received funding from Horizon Europe research and innovation programme under Grant Agreement No.1069890

8. Powder testing and optimisation for selective laser melting additive manufacturing

8.1 Introduction

Selective Laser Melting SLM (or Powder Bed Laser Fusion) is an advanced additive manufacturing (AM) technology that enables the creation of high-precision metal parts. The process involves spreading a thin layer of metallic powder over a build platform and then using a high-powered laser to selectively melt and fuse the powder particles together, based on a digital 3D model. This process is repeated layer by layer until the entire object is formed. Figure 23 and Figure 24 show the SLM equipment available at CSIC and used for the 3D printing of the samples.

SLM is renowned for producing parts with excellent mechanical properties and high density, making it ideal for applications in aerospace, medical, automotive, and other industries where high strength and accuracy are essential. The technology allows for complex geometries that are difficult or impossible to achieve with traditional manufacturing methods, enabling innovative designs and lightweight structures.

Selective Laser Melting (SLM) uses fine metallic powders as the primary material for building parts. As discussed previously, these powders are typically spherical in shape and with a uniform size distribution to ensure consistent layering and fusion during the SLM process.

It is important to note that the main printing parameters, such as laser power, scan speed, scan spacing and layer thickness, play a significant role in the SLM process. These parameters have a direct impact on the microstructure and mechanical properties of the AM product. It is therefore essential to select the most appropriate process parameters using optimisation techniques in order to achieve the best result. The microstructure is controlled by a number of factors, including the cooling rate, the formation of the melt pool, the thermal gradient, the laser parameters and the alloy composition. The rapid solidification, the reduced size of the melt pool and the thermal gradient during SLM are responsible for the formation of a fine microstructure. This fine microstructure is the underlying cause of the excellent mechanical properties [22].

Funded by the European Union

Views and opinions expressed are those of the author(s) only and do not necessarily reflect those of the European Union or CINEA. Neither the European Union nor the granting authority can be held responsible for them. This project has received funding from Horizon Europe research and innovation programme under Grant Agreement No.1069890

Figure 23. SLM equipment available at CSIC

Figure 24. Detail of the building chamber.

8.2 SLM with powder produced by Vacuum Induction Melting Inert Gas Atomization

The fraction of the powder with a grain size below 63µm was 3D printed using the Selective Laser Melting (SLM) technique on a Renishaw AM250 with a laser

Funded by the European Union

Views and opinions expressed are those of the author(s) only and do not necessarily reflect those of the European Union or CINEA. Neither the European Union nor the granting authority can be held responsible for them. This project has received funding from Horizon Europe research and innovation programme under Grant Agreement No.1069890

power of 200W and a spot diameter of 70µm. A protective atmosphere of argon with a maximum of 500 ppm O2 was maintained throughout the fabrication of the samples to reduce oxidation during the melting process. A range of energy densities and laser scan speeds were evaluated to achieve the lowest porosity parts described below.

For porosity determination, the fabricated specimens were metallographically prepared. For this preparation, the specimens were embedded in Multifast Bakelite, then ground with progressive grit sandpaper and finally polished with 3 µm diamond paste. The prepared samples were examined under a light microscope and three images of the surface of each sample were taken at x25 and x50 magnification. These photographs were analysed using ImageJ software, from which quantitative results were obtained for the number, size and circularity of the pores, as well as the percentage of porous area. The same samples were then etched with Keller's reagent and characterised by light microscopy and scanning electron microscopy.

Tensile tests and micro-Vickers hardness measurements of the samples were carried out in a universal tensile machine and a durometer. Microhardness was measured as the average of 10 indentations made on each sample at 100 gf load. Tensile tests were performed in triplicate.

To evaluate the processability of this recycled AlSi7 powder for SLM, a two-level factorial design was employed, incorporating hatch point distance, exposure time and hatch distance. A layer thickness of 25 µm and laser power of 200 W were maintained consistently for all specimens. Table 13. Factorial design of the SLM process parameters studied outlines the primary parameters for manufacturing the specimens. Laser speed is calculated as hatch distance divided by exposure time, given that the laser used is pulsed and the movement between points is significantly faster than the time spent in each point. The volumetric energy density is calculated as laser power divided by the product of the laser speed, the layer thickness, and the hatch distance.

Funded by the European Union

Views and opinions expressed are those of the author(s) only and do not necessarily reflect those of the European Union or CINEA. Neither the European Union nor the granting authority can be held responsible for them. This project has received funding from Horizon Europe research and innovation programme under Grant Agreement No.1069890

Table 13. Factorial design of the SLM process parameters studied

sample	Layer thickness (µm)	Power (W)	Hatch Point Distance (µm)	Exposure Time (µs)	Hatch Distance (µm)	Laser speed (m/s)	Energy density (J/mm3)	Measured density (%)	SD Density (%)
1	25.00	200	60.00	160.00	110.00	0.38	193.94	99.8	0.1
2	25.00	200	100.00	160.00	110.00	0.63	116.36	99.97	0.01
3	25.00	200	100.00	120.00	110.00	0.83	87.27	99.91	0.02
4	25.00	200	100.00	120.00	150.00	0.83	64.00	99.5	0.4
5	25.00	200	80.00	140.00	130.00	0.57	107.69	99.98	0.01
6	25.00	200	60.00	160.00	150.00	0.38	142.22	99.92	0.03
7	25.00	200	80.00	140.00	130.00	0.57	107.69	99.92	0.02
8	25.00	200	80.00	140.00	130.00	0.57	107.69	99.86	0.06
9	25.00	200	60.00	120.00	110.00	0.50	145.45	99.96	0.02
10	25.00	200	100.00	160.00	150.00	0.63	85.33	99.65	0.03
11	25.00	200	60.00	120.00	150.00	0.50	106.67	99.86	0.05

Figure 25 shows optical microscopy images of the XZ plane (Z is the building direction) of selected samples after cutting and metallographic preparation. The samples display remarkably high density across the entire range of values studied, with maximum values of 99.55% (porosity of 0.5%) and 99.98% (porosity of 0.02%), as detailed in Table 13. To gain a detailed understanding of the impact of the parameters, the porosity was quantified using the image analysis software ImageJ.

The results show a clear correlation between porosity and hatch distance. The results of the ANOVA analysis indicate a statistically significant correlation between porosity and hatch distance. However, no statistically significant relationship was observed between porosity and exposure time or point distance. This suggests that the energy density range used is sufficient to achieve complete powder fusion, resulting in a sample density above 99.5%.

Funded by the European Union

Views and opinions expressed are those of the author(s) only and do not necessarily reflect those of the European Union or CINEA. Neither the European Union nor the granting authority can be held responsible for them. This project has received funding from Horizon Europe research and innovation programme under Grant Agreement No.1069890

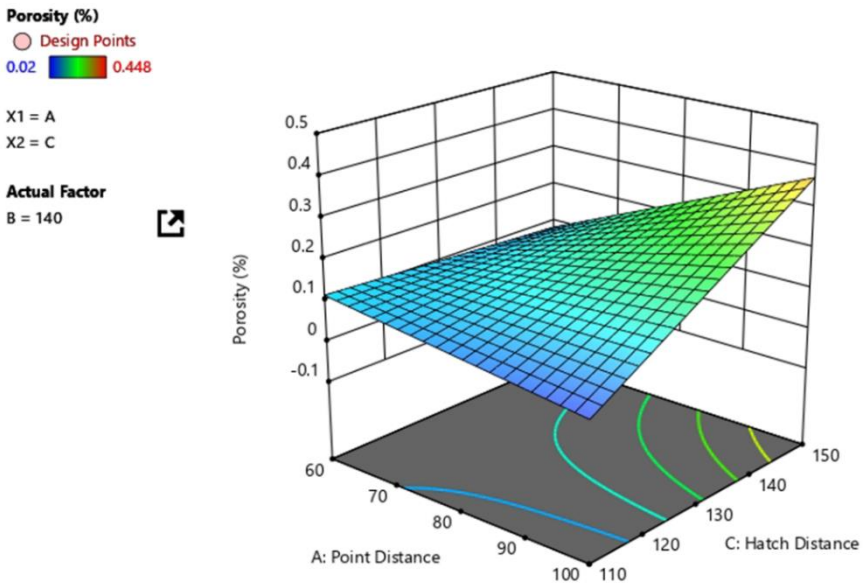

Figure 26 illustrates the response surface of porosity in function of the hatch distance and point distance.

Figure 25. Optical microscopy image (x25) of samples 5, 7 and 8 (Table 4).

Funded by the European Union

Views and opinions expressed are those of the author(s) only and do not necessarily reflect those of the European Union or CINEA. Neither the European Union nor the granting authority can be held responsible for them. This project has received funding from Horizon Europe research and innovation programme under Grant Agreement No.1069890

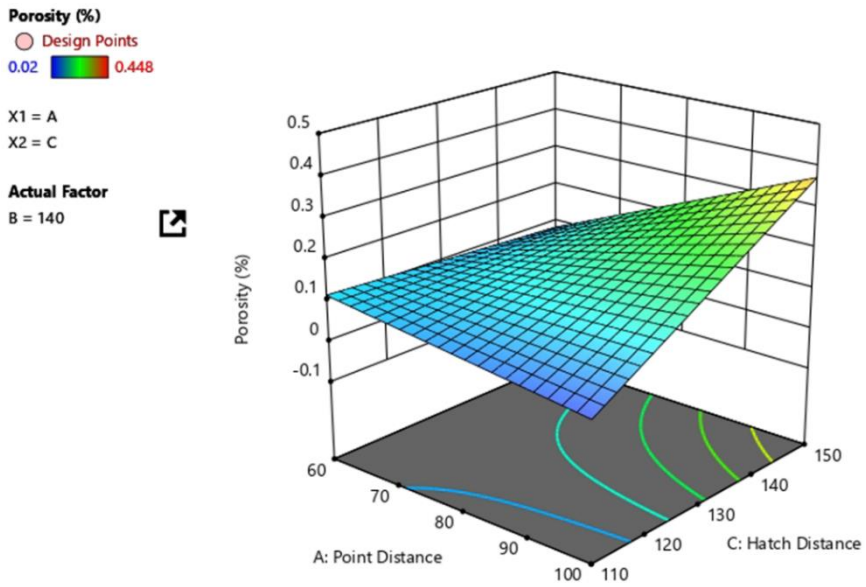

Figure 26. Response surface of the model of porosity in function of Hatch point distance and Hatch distance.

Accordingly, the optimal parameters for achieving the minimum porosity were determined to be a point distance of 80 µm, an exposure time of 140 µm, and a hatch distance of 110 µm. A slightly higher energy density is required to obtain the minimum porosity with the AlSi7 alloy than with the commercial AlSi10Mg powder, which is used in our equipment and set-up. The optimal energy density for the AlSi7 alloy is 127.3 J/mm³, compared to 107.7 J/mm³ for the AlSi10Mg powder. The AlSi7 required slightly more energy for 3D printing, which is to be expected given its greater distance from the eutectic point (approximately 12% Si) and the fact that the melting point of the Al-Si alloy rises from 577°C to 660°C as the wt% Si decreases.

Further specimens were printed in accordance with the specified parameters to enable the characterisation of the mechanical properties, including hardness and tensile testing. Figure 27 illustrates the microstructure obtained with the optimal parameters along the transverse direction of the sample. The microstructure is representative of the as-fabricated AlSi alloys, exhibiting a fish scale-like morphology of molten pools stacked layer by layer [30]. The microstructure is composed of an α-Al solid solution and a network-like Si phase, as illustrated in Figure 28. On an individual specimen basis, the microstructure is consistent throughout. However, each melt pool displays two distinct zones. The first is located at the outer boundary, the second at the centre. The core of the melt pool features a fine microstructure. At the boundary, a coarse dendritic microstructure is visible. The grains here are elongated and larger than in the core. The coarsening of the grains is a result of slower solidification in the boundary region compared to the core. This is a known consequence of the cooling rates being different in different areas [31].

Funded by the European Union

Views and opinions expressed are those of the author(s) only and do not necessarily reflect those of the European Union or CINEA. Neither the European Union nor the granting authority can be held responsible for them. This project has received funding from Horizon Europe research and innovation programme under Grant Agreement No.1069890

On the other hand, the chemical composition obtained is in exact accordance with the target specifications for the AlSi7 alloy, as illustrated inTable 14.

Table 14. Optical Spark chemical composition of printed sample with optimum parameters.

	Si	Fe	Cu	Mn	Mg	Ni	Zn	Ti	Al
%Wt ± SD	7.0±0.1	0.33±0.01	0.48±0.02	0.61±0.01	0.09	0.04	0.01	0.05	Balance

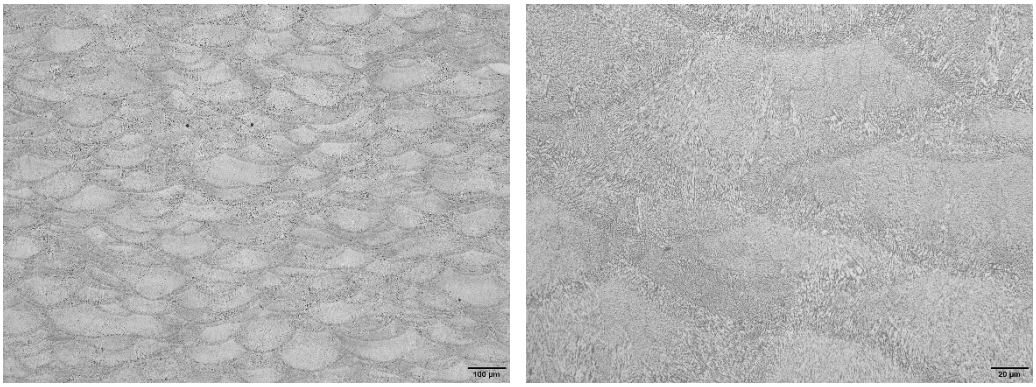

Figure 27. Optical microscopy microstructure of the samples (x200 and x1000)

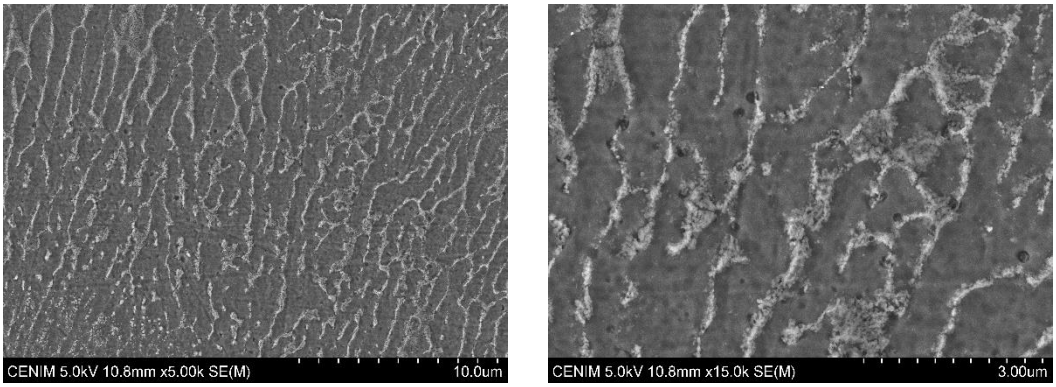

Figure 28. Scanning electron microscope image of the typical microstructure obtained (x5000 and x15000).

Two types of heat treatments have been documented in the literature on AlSi AM samples. The first is solution heat treatment, which involves temperatures between 450 and 550 °C, followed by an ageing treatment between 150 and 180 °C. The second is annealing (stress relieving) at 300 °C for two hours [22]. It has been demonstrated that heat treatment at elevated temperatures results in a notable decrease in both tensile and yield strengths, while also increasing ductility. The annealing treatment produces outcomes that are not significantly different from those of the solution heat treatment, effectively eliminating residual stresses and enhancing ductility. The AlSi7 specimens produced in

Funded by the European Union

Views and opinions expressed are those of the author(s) only and do not necessarily reflect those of the European Union or CINEA. Neither the European Union nor the granting authority can be held responsible for them. This project has received funding from Horizon Europe research and innovation programme under Grant Agreement No.1069890

this study were characterised in their as-built state and compared with existing literature on AlSi alloys in the same state.

The average hardness of the AM samples is 105 ± 5 (HV0.5). The value is slightly lower than that of AlSi7Mg and AlSi10Mg obtained by SLM. However, it should be noted that the absence of Mg in this alloy means that the typical hardening of Al-Si-Mg alloys by solid diffusion of Mg in the Al matrix does not occur. The fine dispersion of Si in the Al phase results in a very high Vickers hardness of the as-built AlSi10Mg SLM parts, namely 127 ± 3 (HV0.5). In our case, the as-built AlSi7 reaches values comparable to those of the AlSi10Mg obtained by high-pressure die casting (95–105 HV) [31].

Figure 29 shows the tensile test results for a sample printed using the optimal parameters. The average ultimate tensile strength (UTS) measured was 357 ± 6 MPa, with an elongation of 2.4 ± 0.3%. This result is slightly lower than the reported values of 396 ± 8 MPa and 5.5% elongation for as-built AlSi10Mg, as provided by reference [32], but is in close alignment with the values of 359 MPa and 1.7% reported also for as-built AlSi10Mg, as reported by reference[33]. In a study by Parveen et al. [34], the impact of printing parameters on the microstructure and tensile properties of AM AlSi10Mg alloy was investigated, with the factors being layer thickness, laser power, and scan velocity. The most favourable outcomes were observed with lower porosity and a superfine cellular dendritic microstructure, achieving a UTS of 446 MPa and an elongation of 9.63%. Regardless, the results obtained with the recycled AlSi7 powder are demonstrably superior to the mechanical properties of cast AlSi (UTS 300-320 MPa).

Funded by the European Union

Views and opinions expressed are those of the author(s) only and do not necessarily reflect those of the European Union or CINEA. Neither the European Union nor the granting authority can be held responsible for them. This project has received funding from Horizon Europe research and innovation programme under Grant Agreement No.1069890

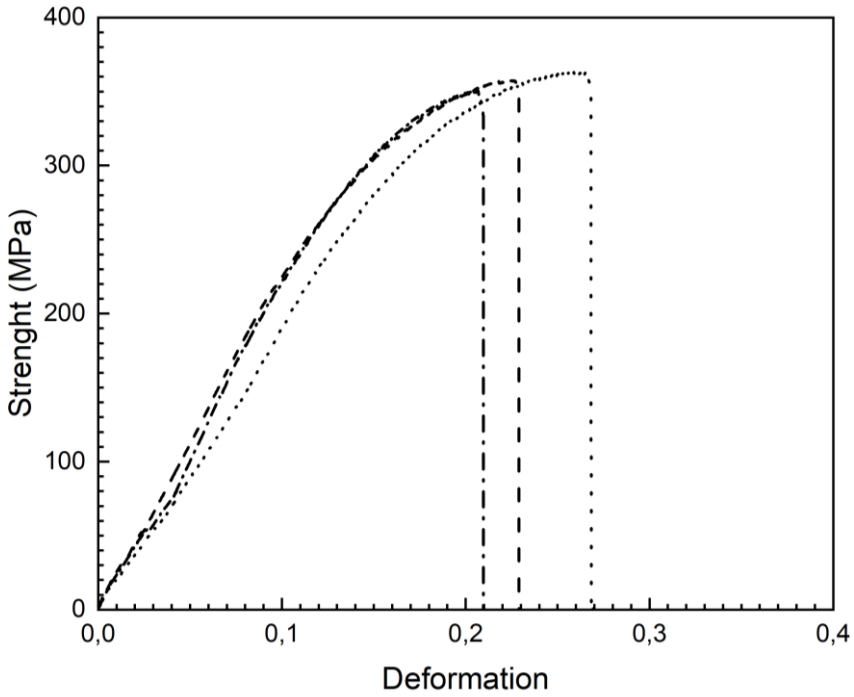

Figure 29. Tensile deformation curves of the optimised samples, per triplicate.

8.3 SLM with powder produced by Centrifugal Atomization

Selective Laser Melting (SLM) was used also on the Renishaw AM250 with a laser power of 200W and a spot diameter of 70 µm to 3D print the fraction of the powder below 63 µm available at CSIC. To reduce oxidation during the melting process, a protective atmosphere of argon with a maximum of 500 ppm O2 was maintained throughout the fabrication of the samples.

For porosity determination, the fabricated specimens were metallographically prepared and examined under a light microscope, and three images of the surface of each sample were taken at x25 and x50 magnification. These photographs were analysed using ImageJ software, from which quantitative results were obtained for the percentage of porous area. The same samples were then etched with Keller's reagent and characterised by light microscopy.

To evaluate the processability of this recycled AlSi7Mg powder for SLM, the same initial two-level factorial design used for AlSi7 powder produced by VIGA atomisation was employed, incorporating hatch point distance, exposure time and hatch distance. A layer thickness of 25 µm and laser power of 200 W were maintained consistently for all specimens. Table 15 outlines the primary

Funded by the European Union

Views and opinions expressed are those of the author(s) only and do not necessarily reflect those of the European Union or CINEA. Neither the European Union nor the granting authority can be held responsible for them. This project has received funding from Horizon Europe research and innovation programme under Grant Agreement No.1069890

parameters for manufacturing the specimens. Laser speed is calculated as hatch distance divided by exposure time, given that the laser used is pulsed and the movement between points is significantly faster than the time spent in each point. The volumetric energy density is calculated as laser power divided by the product of the laser speed, the layer thickness, and the hatch distance.

Table 15. Factorial design of the SLM process parameters studied

sample	Layer thickness (µm)	Power (W)	Hatch Point Distance (µm)	Exposure Time (µs)	Hatch Distance (µm)	Laser speed (m/s)	Energy density (J/mm3)	Measured density (%)	SD Density (%)
1	25.00	200	60.00	160.00	110.00	0.38	193.94	99.88	0.08
2	25.00	200	100.00	160.00	110.00	0.63	116.36	99.94	0.06
3	25.00	200	100.00	120.00	110.00	0.83	87.27	99.98	0.00
4	25.00	200	100.00	120.00	150.00	0.83	64.00	99.81	0.05
5	25.00	200	80.00	140.00	130.00	0.57	107.69	99.98	0.01
6	25.00	200	60.00	160.00	150.00	0.38	142.22	99.95	0.02
7	25.00	200	80.00	140.00	130.00	0.57	107.69	99.93	0.00
8	25.00	200	80.00	140.00	130.00	0.57	107.69	99.93	0.01
9	25.00	200	60.00	120.00	110.00	0.50	145.45	99.96	0.01
10	25.00	200	100.00	160.00	150.00	0.63	85.33	99.97	0.01
11	25.00	200	60.00	120.00	150.00	0.50	106.67	99.98	0.01

Figure 30 shows optical microscopy images of the XZ plane (Z is the building direction) of selected samples after cutting and metallographic preparation. The samples display remarkably high density across the entire range of values studied, with values from 99.81% to 99,98% as detailed inTable 15, where is shown the quantified density using the image analysis software ImageJ.

No correlation is appreciable between the SLM process parameters studied and the sample density. This indicates that the energy density range and laser scan speed used is sufficient to achieve complete powder fusion, resulting in a sample density above 99.9%. Only the samples processed with the maximum (194 J/mm3) and minimum (64 J/mm3) energy density shows a slightly lower value of the density of 99.8%.

Funded by the European Union

Views and opinions expressed are those of the author(s) only and do not necessarily reflect those of the European Union or CINEA. Neither the European Union nor the granting authority can be held responsible for them. This project has received funding from Horizon Europe research and innovation programme under Grant Agreement No.1069890

Figure 30. Optical microscopy image (x25) of samples 3, 5 and 11 (Table X).

Figure 31 illustrates the typical microstructure obtained along the transverse direction of the sample. The microstructure is again representative of the as-fabricated AlSi alloys, exhibiting a fish scale-like morphology of molten pools stacked layer by layer. The microstructure is composed of an α-Al solid solution and a network-like Si phase. The microstructure is consistent from sample to sample. However, there are two distinct zones in each melt pool. The core of the melt pool is characterised by a fine grain structure. At the edge of the pool a coarse dendritic microstructure can be seen with elongated and larger grains. As discussed previously the coarsening of the grains is caused by slower solidification at the boundary compared to the core.

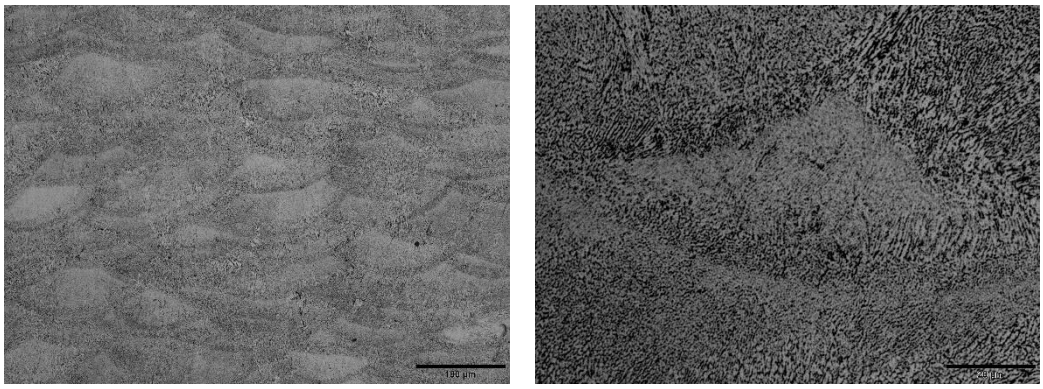

Figure 31. Typical optical microscopy microstructure of the samples (x200 and x1000)

The average hardness of the samples 3D printed with AlSi7Mg from centrifugal atomisation is 118 ± 6 (HV0.5). The value is higher than that of AlSi7 obtained by VIGA atomisation, which shows the hardening effect of Mg as previously discussed. This value is very close to the typical AlSi10Mg value obtained by other authors by SLM and remarkable higher to those of the AlSi10Mg obtained by high-pressure die casting (95–105 HV) [31].

Funded by the European Union

Views and opinions expressed are those of the author(s) only and do not necessarily reflect those of the European Union or CINEA. Neither the European Union nor the granting authority can be held responsible for them. This project has received funding from Horizon Europe research and innovation programme under Grant Agreement No.1069890

9. Conclusions

This study examines the potential of recycling aluminium alloys from EV battery packs for use in additive manufacturing (AM), with a focus on selective laser melting (SLM).

A real battery pack case was disassembled into its constituent components, and the different aluminium alloys present were identified as AlSi12, 5xxx, 3xxx and 6xxx series. The alloys were successfully grouped, melted and remixed to form an AlSi7 alloy, targeted and suitable for SLM.

The production of powder by Inert Gas Atomization of the recycled aluminium resulted in a powder with a particle size distribution appropriate for SLM, particularly in the < 63 µm range. The morphology was predominantly spherical and the internal structure was free of significant pores, indicating that the material is of a quality appropriate for AM purposes.

The production of AlSi7 powder by Centrifugal Atomization of the recycled aluminium resulted in powder suitable for additive manufacturing processes. obtaining spherical powder without satellites. For Cu powder production extra tests using recovered metal are required to set-up the technology, although powder obtained for initial tests are suitable for additive manufacturing.

A factorial design study identified the optimal SLM parameters to minimise porosity and achieve densities above 99.9% using the both powders produced by VIGA Atomisation and Centrifugal Atomisation. The optimum requires a slightly higher energy density than that of used for commercial AlSi10Mg powders but all the range of energy density and scan laser speed offer a superb density. In other words, the SLM process has proven to be very robust around this optimum for the production of fully dense parts.

In both cases the atomised powder was sieved and only the < 63 µm range was used and no statistical significance differences was observed in the resulting sample density with SLM optimum parameters.

The composition of the obtained parts reveals a higher proportion of Fe than that observed in SLM parts made from commercial powder. However, the as-built microstructure of the printed AlSi7 alloy demonstrated typical fine microstructures with distinct melt pool boundaries and the absence of detrimental AlSiFe precipitates. The mechanical testing demonstrated that the hardness values (105±5 HV) with powder of AlSi7 were slightly lower than those of AlSi10Mg due to the absence of magnesium, but the hardness obtained with powder of composition AlSi7Mg (118±6 HV) increases. The ultimate tensile strength and % elongation values were within the range of those typically observed in SLM-produced AlSi alloys. Further work is required to investigate

Funded by the European Union

Views and opinions expressed are those of the author(s) only and do not necessarily reflect those of the European Union or CINEA. Neither the European Union nor the granting authority can be held responsible for them. This project has received funding from Horizon Europe research and innovation programme under Grant Agreement No.1069890

the evolution of these alloys rich in Fe impurities during heat treatments to improve their ductility.

The results confirm the feasibility of using recycled aluminium from EV battery packs for high quality AM applications. This approach not only provides a sustainable method of reusing valuable materials, but also reduces the environmental impact associated with primary aluminium production.

Moreover, VIGA atomisation and Centrifugal Atomisation have proven to be able to produce powder of suitable quality for SLM from aluminium and copper recovered from battery pack cases.

This study opens up new opportunities for further optimisation in the recycling of aluminium alloys from EV battery packs for use in AM as a promising sustainable practice. These results reinforce the objectives of recovery of valuable materials (metal oxides, plastics and metals) from spent LIBs through different recycling techs. The obtained materials can be re-used in 3D manufacturing within the batt value chain or used in alternative uses.

10. References

[1] A.M. Lewis, J.C. Kelly, G.A. Keoleian, Vehicle lightweighting vs. electrification: Life cycle energy and GHG emissions results for diverse powertrain vehicles, Appl. Energy 126 (2014) 13–20. https://doi.org/10.1016/j.apenergy.2014.03.023.

[2] Y. Xiong, Y. Pan, L. Wu, B. Liu, Effective weight-reduction- and crashworthiness-analysis of a vehicle's battery-pack system via orthogonal experimental design and response surface methodology, Eng. Fail. Anal. 128 (2021) 105635. https://doi.org/10.1016/j.engfailanal.2021.105635.

[3] J. Wen, D. Zhao, C. Zhang, An overview of electricity powered vehicles: Lithium-ion battery energy storage density and energy conversion efficiency, Renew. Energy 162 (2020) 1629–1648. https://doi.org/10.1016/j.renene.2020.09.055.

[4] A. Aversa, G. Marchese, A. Saboori, E. Bassini, D. Manfredi, S. Biamino, D. Ugues, P. Fino, M. Lombardi, New Aluminum Alloys Specifically Designed for Laser Powder Bed Fusion: A Review, Materials 12 (2019) 1007. https://doi.org/10.3390/ma12071007.

[5] L. Lander, C. Tagnon, V. Nguyen-Tien, E. Kendrick, R.J.R. Elliott, A.P. Abbott, J.S. Edge, G.J. Offer, Breaking it down: A techno-economic assessment of the impact of battery pack design on disassembly costs, Appl. Energy 331 (2023) 120437. https://doi.org/10.1016/j.apenergy.2022.120437.

[6] L. Yun, D. Linh, L. Shui, X. Peng, A. Garg, M.L.P. Le, S. Asghari, J. Sandoval, Metallurgical and mechanical methods for recycling of lithium-ion battery pack for electric

Funded by the European Union

Views and opinions expressed are those of the author(s) only and do not necessarily reflect those of the European Union or CINEA. Neither the European Union nor the granting authority can be held responsible for them. This project has received funding from Horizon Europe research and innovation programme under Grant Agreement No.1069890

vehicles, Resour. Conserv. Recycl. 136 (2018) 198–208. https://doi.org/10.1016/j.resconrec.2018.04.025.

[7] K. Wegener, W.H. Chen, F. Dietrich, K. Dröder, S. Kara, Robot Assisted Disassembly for the Recycling of Electric Vehicle Batteries, Procedia CIRP 29 (2015) 716–721. https://doi.org/10.1016/j.procir.2015.02.051.

[8] D. Raabe, C.C. Tasan, E.A. Olivetti, Strategies for improving the sustainability of structural metals, Nature 575 (2019) 64–74. https://doi.org/10.1038/s41586-019-1702-5.

[9] D. Raabe, D. Ponge, P.J. Uggowitzer, M. Roscher, M. Paolantonio, C. Liu, H. Antrekowitsch, E. Kozeschnik, D. Seidmann, B. Gault, F. De Geuser, A. Deschamps, C. Hutchinson, C. Liu, Z. Li, P. Prangnell, J. Robson, P. Shanthraj, S. Vakili, C. Sinclair, L. Bourgeois, S. Pogatscher, Making sustainable aluminum by recycling scrap: The science of “dirty” alloys, Prog. Mater. Sci. 128 (2022) 100947. https://doi.org/10.1016/j.pmatsci.2022.100947.

[10] R. Modaresi, A.N. Løvik, D.B. Müller, Component- and Alloy-Specific Modeling for Evaluating Aluminum Recycling Strategies for Vehicles, JOM 66 (2014) 2262–2271. https://doi.org/10.1007/s11837-014-0900-8.

[11] S. Pogatscher, H. Antrekowitsch, M. Werinos, G. Rank, A. Kais, R. Prillhofer, J.F. Loffler, P.J. Uggowitzer, Statistical and Thermodynamic Optimization of Trace-Element Modified Al-Mg-Si-Cu Alloys, in: Light Met. 2015, John Wiley & Sons, Ltd, 2015: pp. 263–270. https://doi.org/10.1002/9781119093435.ch45.

[12] D. Wang, T. Zhang, X. Guo, D. Ling, L. Hu, G. Jiang, The potential of 3D printing in facilitating carbon neutrality, J. Environ. Sci. 130 (2023) 85–91. https://doi.org/10.1016/j.jes.2022.10.024.

[13] S. Graziosi, J. Faludi, T. Stanković, Y. Borgianni, N. Meisel, S.I. Hallstedt, D.W. Rosen, A vision for sustainable additive manufacturing, Nat. Sustain. 7 (2024) 698–705. https://doi.org/10.1038/s41893-024-01313-x.

[14] M. Gebler, A.J.M. Schoot Uiterkamp, C. Visser, A global sustainability perspective on 3D printing technologies, Energy Policy 74 (2014) 158–167. https://doi.org/10.1016/j.enpol.2014.08.033.

[15] P.C. Priarone, V. Lunetto, E. Atzeni, A. Salmi, Laser powder bed fusion (L-PBF) additive manufacturing: On the correlation between design choices and process sustainability, Procedia CIRP 78 (2018) 85–90. https://doi.org/10.1016/j.procir.2018.09.058.

[16] E.A. Jägle, Z. Sheng, L. Wu, L. Lu, J. Risse, A. Weisheit, D. Raabe, Precipitation Reactions in Age-Hardenable Alloys During Laser Additive Manufacturing, JOM 68 (2016) 943–949. https://doi.org/10.1007/s11837-015-1764-2.

Funded by the European Union

Views and opinions expressed are those of the author(s) only and do not necessarily reflect those of the European Union or CINEA. Neither the European Union nor the granting authority can be held responsible for them. This project has received funding from Horizon Europe research and innovation programme under Grant Agreement No.1069890

[17] F.H. Froes, Y.-W. Kim, S. Krishnamurthy, Rapid solidification of lightweight metal alloys, Mater. Sci. Eng. A 117 (1989) 19–32. https://doi.org/10.1016/0921-5093(89)90082-8.

[18] J. Suchy, L. Pantelejev, D. Palousek, D. Koutny, J. Kaiser, Processing of AlSi9Cu3 alloy by selective laser melting, Powder Metall. 63 (2020) 197–211. https://doi.org/10.1080/00325899.2020.1792675.

[19] S. Yamasaki, T. Okuhira, M. Mitsuhara, H. Nakashima, J. Kusui, M. Adachi, Effect of Fe Addition on Heat-Resistant Aluminum Alloys Produced by Selective Laser Melting, Metals 9 (2019) 468. https://doi.org/10.3390/met9040468.

[20] H. Kaufmann, W. Fragner, H. Suppan, A.B. Spierings, P.J. Uggowitzer, A. Schubert, M. Hummel, Starting material, use thereof, and additive manufacturing process using said starting material, US11597984B2, 2023. https://patents.google.com/patent/US11597984B2/en (accessed July 24, 2023).

[21] S. Sun, L. Zheng, Y. Liu, J. Liu, H. Zhang, Characterization of Al–Fe–V–Si heat-resistant aluminum alloy components fabricated by selective laser melting, J. Mater. Res. 30 (2015) 1661–1669. https://doi.org/10.1557/jmr.2015.110.

[22] R.E. Gite, V.D. Wakchaure, A review on process parameters, microstructure and mechanical properties of additively manufactured AlSi10Mg alloy, Mater. Today Proc. 72 (2023) 966–986. https://doi.org/10.1016/j.matpr.2022.09.100.

[23] I. Polmear, D.S. John, J.F. Nie, M. Qian, Light Alloys: Metallurgy of the Light Metals, Academic Press, 2017. https://research.monash.edu/en/publications/light-alloys-metallurgy-of-the-light-metals (accessed May 28, 2024).

[24] X. Liu, C. Wang, S.-Y. Zhang, J.-W. Song, X.-L. Zhou, M. Zha, H.-Y. Wang, Fe-bearing phase formation, microstructure evolution, and mechanical properties of Al-Mg-Si-Fe alloy fabricated by the twin-roll casting process, J. Alloys Compd. 886 (2021) 161202. https://doi.org/10.1016/j.jallcom.2021.161202.

[25] A. Fortini, M. Merlin, E. Fabbri, S. Pirletti, G.L. Garagnani, On the influence of Mn and Mg additions on tensile properties, microstructure and quality index of the A356 aluminum foundry alloy, Procedia Struct. Integr. 2 (2016) 2238–2245. https://doi.org/10.1016/j.prostr.2016.06.280.

[26] G. Piscopo, E. Atzeni, A. Saboori, A. Salmi, An Overview of the Process Mechanisms in the Laser Powder Directed Energy Deposition, Appl. Sci. 13 (2023) 117. https://doi.org/10.3390/app13010117.

[27] X. Li, Q. Zhu, S. Shu, J. Fan, S. Zhang, Fine spherical powder production during gas atomization of pressurized melts through melt nozzles with a small inner diameter, Powder Technol. 356 (2019) 759–768. https://doi.org/10.1016/j.powtec.2019.09.023.

Funded by the European Union

Views and opinions expressed are those of the author(s) only and do not necessarily reflect those of the European Union or CINEA. Neither the European Union nor the granting authority can be held responsible for them. This project has received funding from Horizon Europe research and innovation programme under Grant Agreement No.1069890

[28] A. Averardi, C. Cola, S.E. Zeltmann, N. Gupta, Effect of particle size distribution on the packing of powder beds: A critical discussion relevant to additive manufacturing, Mater. Today Commun. 24 (2020) 100964. https://doi.org/10.1016/j.mtcomm.2020.100964.

[29] C.D. Boley, S.A. Khairallah, A.M. Rubenchik, Calculation of laser absorption by metal powders in additive manufacturing, Appl. Opt. 54 (2015) 2477–2482. https://doi.org/10.1364/AO.54.002477.

[30] H. Tang, C. Gao, Y. Zhang, N. Zhang, C. Lei, Y. Bi, P. Tang, J.H. Rao, Effects of direct aging treatment on microstructure, mechanical properties and residual stress of selective laser melted AlSi10Mg alloy, J. Mater. Sci. Technol. 139 (2023) 198–209. https://doi.org/10.1016/j.jmst.2022.08.032.

[31] L. Thijs, K. Kempen, J.-P. Kruth, J. Van Humbeeck, Fine-structured aluminium products with controllable texture by selective laser melting of pre-alloyed AlSi10Mg powder, Acta Mater. 61 (2013) 1809–1819. https://doi.org/10.1016/j.actamat.2012.11.052.

[32] K. Kempen, L. Thijs, J. Van Humbeeck, J.-P. Kruth, Mechanical Properties of AlSi10Mg Produced by Selective Laser Melting, Phys. Procedia 39 (2012) 439–446. https://doi.org/10.1016/j.phpro.2012.10.059.

[33] A. Mauduit, S. Pillot, F. Frascati, Application study of AlSi10Mg alloy by selective laser melting: physical and mechanical properties, microstructure, heat treatments and manufacturing of aluminium metallic matrix composite (MMC), Metall. Res. Technol. 112 (2015) 605. https://doi.org/10.1051/metal/2015039.

[34] S. Parveen, R.S.U. Rao, D. K, G. Telasang, Investigation on Correlation between Microstructure and Mechanical Properties of Alsi10Mg Specimens by AM Technology, (2021). https://doi.org/10.2139/ssrn.3989415.

Funded by the European Union

Views and opinions expressed are those of the author(s) only and do not necessarily reflect those of the European Union or CINEA. Neither the European Union nor the granting authority can be held responsible for them. This project has received funding from Horizon Europe research and innovation programme under Grant Agreement No.1069890